PHYSICAL REVIEW D VOLUME 18, NUMBER 5 1 SEPTEMBER 1978

Phenomenology of high-momentum-transfer elastic processes

D. D. Coon
University of Pittsburgh, Pittsburgh, Pennsylvania 15213

J. F. Gunion
University of California, Davis, California 95616

J. Trân Thanh Vân
University Paris-Sud, Orsay, France, 91405

R. Blankenbecler
Stanford Linear Accelerator Center, Stanford University, Stanford, California 94305
(Received 14 November 1977)

An analysis is carried out to extract the leading effective trajectories and residues in pp and $\pi^- p$ elastic scattering. The results are compared with the predictions of the constituent-interchange model and the logarithmic dual model, which are shown to be the only two types of theory capable of providing a uniform link between backward and forward Regge regions and the fixed-angle region. The hypothesis of a smooth connection between forward and backward Regge regions puts strong contraints on *a priori* unrelated trajectories and residues. The possibility of a connection between the two models is discussed. As expected from interchange theory the extracted $\pi^- p$ trajectory and residue behave quite differently than those for pp. The dual model seems to give the best overall description of the pp trajectory and residue functions while the πp results agree completely with the interchange predictions. The two model fits to pp elastic scattering at moderate energies (12–24 GeV) are used to extract an expected Pomeron term. The shape of the extracted diffractive contribution is strikingly similar to the recent CERN ISR differential cross sections which exhibit a dip at $t = -1.4$ GeV^2 and a slow falloff in the large-t region.

I. INTRODUCTION

Recently there has been a great deal of interest in large-momentum-transfer processes. Two of the more successful theoretical approaches have been those of the constituent-interchange model (CIM)[1-4] and of the logarithmic-trajectory dual model (LDM).[5] The parton-interchange theory provides a good description of all experimentally measured large-angle exclusive scattering processes; the dual model has been shown to provide a precise fit to the nondiffractive component of pp elastic scattering at all angles.[6,7]

In both theories the fixed-angle behavior provides a smooth link between forward and backward Regge behavior. However, they differ in their predictions at higher energies and momentum transfers. The LDM predicts, for instance, that the effective Regge trajectory falls logarithmically for all momentum transfers, while the CIM predicts that the effective trajectory should approach a calculable, process-dependent, constant (provided the form factors have fixed power law falloff).

In this paper we analyze the pp and πp elastic scattering data extracting effective trajectories and residue functions. For this purpose it is very important to distinguish between

$$s^{\alpha(t)} \quad \text{and} \quad (-u)^{\alpha(t)} \tag{1}$$

in order to treat the large-momentum-transfer region properly. The results are then compared to the predictions of the two theories. In addition we complement the two models by including a Pomeron contribution and in each case present a fit to the full momentum-transfer range of pp elastic scattering. Having performed this fit at low energies, s below 60 GeV^2, the resulting Pomeron extrapolates very well to CERN ISR energies.

II. PROPERTIES OF THE CIM AND LDM

In this section we will review the properties of the parton-interchange and logarithmic dual models with emphasis upon their predictions for asymptotic effective trajectories and residue functions. (See also Ref. 3.) We begin by demonstrating that the interchange and logarithmic-trajectory models are the only ones that provide a uniform fixed-angle link between forward and backward Regge behavior. The argument is essentially the same as that given by Arik.[8] In general, of course, the non-Pomeron part of the cross section could be the sum of two unrelated terms,

$$\frac{d\sigma^{\text{non-Pomeron}}}{dt} = \frac{d\sigma^{\text{forward}}}{dt} + \frac{d\sigma^{\text{fixed angle}}}{dt},$$

the forward piece dominating at small angle, fixed t while the second piece dominates the fixed-large-angle regime. However, it is an attractive possibility that there is only one analytic term which smoothly connects both regions, and it is amusing that the solutions to this criterion are so restricted.

Consider an exotic s-channel amplitude. For small $(-t)$ and large $(-u)$ the leading asymptotic term is presumed to have the standard Regge form

$$\beta_t(t)(-u)^{\alpha_t(t)}\,, \tag{2}$$

whereas for large $(-t)$ and small $(-u)$ (i.e., in the backward direction) the leading term is

$$\beta_u(u)(-t)^{\alpha_u(u)}. \tag{3}$$

[Throughout this paper we define the Regge form to have scale factor = 1. Any power dependence of $\beta(t)$ can be absorbed by choice of a different scale factor.] If one now requires[8] that the fixed-angle amplitude be obtained either as the large t limit of the forward Regge form or as the large u limit of the backward Regge form we obtain

$$\beta_t(t)(-u)^{\alpha_t(t)} = \beta_u(u)(-t)^{\alpha_u(u)}\,, \tag{4}$$

when both t and u are asymptotic. The only solution to this functional equation is

$$\beta_t(t)(-u)^{\alpha_t(t)} \equiv \beta_0(-t/t_0)^{\alpha_u(-u_0)}(-u/u_0)^{\alpha_t(t)}\,, \tag{5}$$

with

$$\alpha_t(t) = \alpha_t(-t_0) - d\ln(-t/t_0)\,,$$

with the u-channel results obtained by $t \longleftrightarrow u$ interchange. If nonleading contributions are also considered, the trajectories become more general functions of t but approach the above form at large t (Ref. 9).

The general result with a nonzero d corresponds to a logarithmically decreasing trajectory (as in the dual-model amplitude), while the special case with $d = 0$ is the prediction of interchange theory that all trajectories approach a constant at large negative t. In addition we see from Eq. (5) that $\beta_t(t)$ of Eq. (4) has the form

$$\beta_t(t) = \beta_0(-t/t_0)^{\alpha_u(-1)}(u_0)^{-\alpha_t(-t_0)}\,. \tag{6}$$

That is, the effective residue function for, say, the t channel, is an increasing or decreasing function of negative t depending upon whether or not the crossed-channel trajectory, extrapolated to -1 using the forms of Eq. (5), is positive or negative. In particular, for the interchange case, in which effective trajectories are negative asymptotically, the residue function always decreases for increasing (asymptotic) negative t. Nonasymptotic corrections can have a considerable effect,

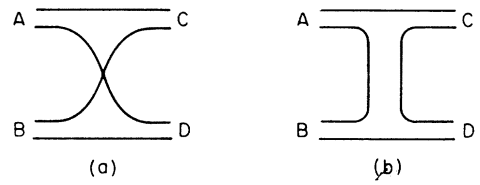

FIG. 1. (a) Interchange topology—ut diagram. (b) Interchange topology—st diagram.

however. In practice, the asymptotic interchange amplitude can take the form (up to logarithmic modifications) of a sum of two such terms, both of which are important at fixed angles with only one dominant in the "Regge" regions (the coupled-channel problem exhibits this behavior[10]), or the form of a convolution integral which reduces to Eq. (5) (with $d = 0$) in either "Regge" region.

The interchange contribution to bound-state scattering is depicted in Fig. 1(a), the two scattering states simply interchange two of their respective fundamental constituents. In many respects this is the simplest possible theory of deep-elastic scattering since, for simple wave functions, it requires a knowledge only of the form factors of the colliding particles, and not a detailed understanding of the underlying forces which bind the constituents together to form the physical hadrons. Furthermore, constituent interchange inevitably occurs in any composite model of the hadrons.

To the extent that it is not necessary to explicitly exhibit vector gluons (or other binding forces) either because of a weak coupling constant or some type of selection rule, Reggeization in the small-angle region must proceed via t-channel iteration of the interchange amplitude. This is discussed in detail in Ref. 10. On the other hand, vector gluon exchanges (such as those depicted in Fig. 2) could well result in the Reggeization of the scattering amplitude.[11] Since this type of Reggeization preserves the topology of the usual duality diagrams, one might expect that there exists a dual amplitude with Regge behavior which in the limit of weak gluon coupling strength reduces to the parton-interchange amplitude.

If in analogy with the Coulomb trajectory[11] one identifies the coefficient d as being proportional

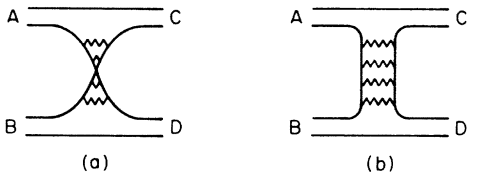

FIG. 2. (a) ut and (b) st vector-gluon-exchange diagrams which could contribute to Reggeization.

to the coupling constant $(g^2/4\pi)$, then we shall show that the dual amplitude discussed here does, in general, reduce to the form of an interchange amplitude in a particular limit.

We begin by reviewing the general form of the interchange contribution to deep-elastic hadronic scattering. The $(u\text{-}t)$ topology contribution, Fig. 1(a), to the invariant scattering amplitude, $M(s,t,u)$ for hadrons composed of two spinless constituents may in the simplest[12] covariant model be expressed in the form

$$M(s,t,u)\propto\int_0^1 dx\, N_B(x)[xu+(1-x)t]\psi_A(xu+(1-x)t)\times\psi_C(xu)\psi_D((1-x)t)\,, \tag{7}$$

with

$$N_B(x)\propto\theta\left(x-\tfrac{1}{2}\right)(1-x)^{B-1}+\theta\left(\tfrac{1}{2}-x\right)x^{B-1}\,.$$

For asymptotic values of $t\gg u\gg m^2$, this reduces to

$$M\propto(-t)^{1-D-A}(-u)^{-C},\quad B>D+A-1$$
$$\propto(-t)^{-B}(-u)^{1-C-A},\quad B<D+A-1\,, \tag{8}$$

while for $u\gg t\gg m^2$,

$$M\propto(-u)^{1-C-A}(-t)^{-B},\quad B>C+A-1$$
$$\propto(-u)^{-B}(-t)^{1-A-D},\quad B<C+A-1\,, \tag{9}$$

where ψ_A, which describes the breakup of particle A into its constituents, behaves asymptotically as $1/t^A$. Up to possible logarithmic modifications, this same power law characterizes particle A's electromagnetic form factor, $F_A(t)\propto 1/t^A$ if the hadronic constituents are pointlike. This expression must be symmetrized in the particles A, B, C, and D. In the case of identical-particle scattering, there are additional singular end-point contributions and we obtain (for $u\gg t\gg m^2$) by keeping both N_B terms

$$M\propto\left[\frac{\ln(-u)}{(-u)^B}(-t)^{1-2B}+\frac{\ln(-t)}{(-t)^B}(-u)^{1-2B}\right], \tag{10}$$

with the result for $t\gg u\gg m^2$ obtained by $t\longleftrightarrow u$ interchange. A particularly important example is that of p-p scattering which corresponds to $B=2$ (dipole form factor for the proton) for which we obtain

$$\frac{d\sigma}{dt}\propto\frac{1}{(tu)^6}\left[\frac{u\ln(-u)+t\ln(-t)}{s}\right]^2 \tag{11}$$

as an adequate approximation for arbitrary (asymptotic) t and u. If we neglect the logarithmic modifications in the region of 90°, this is equivalent to

$$\frac{d\sigma}{dt}\propto\frac{1}{s^{12}}\frac{1}{(1-z^2)^6}\,. \tag{12}$$

The above discussion has assumed that only $(u-t)$ topology graphs contribute to p-p scattering. This is certainly the case if, as argued elsewhere, only valence quarks are present in the proton's wave function at high transverse momentum.

The effects of spin complications and more detailed dimensional-counting models for the proton[14] can be significant. A detailed calculation in such a model yields fixed-angle $1/s^{10}$ behavior with angular behavior of $1/(1-z^2)^6$, i.e.,

$$\frac{d\sigma}{dt}\propto\frac{1}{s^{10}}\frac{1}{(1-z^2)^6}\,.$$

The $1/s^{10}$ result depends upon assuming no pairing of quarks in the proton wave function; if the $\mathfrak{N}$ quark is paired to one of the $\mathcal{P}$ quarks (as deep-inelastic data may be indicating) the two-particle approximation used in deriving Eq. (12) is valid and $1/s^{12}$ behavior results. Theoretical models involving specific vector-gluon diagrams which preserve the $\mathcal{P}\mathfrak{N}$ quark pairing within the interchange diagram can be used to verify this result.

Equation (12) and especially the spin-$\frac{1}{2}$ dimensional-counting result are in fact quite close to the fixed-angle fit proposed by Landshoff and Polkinghorne[15]

$$\frac{d\sigma}{dt}\propto\frac{1}{s^{10}}\frac{1}{(1-z^2)^7}\,. \tag{13}$$

For the quark-pairing case, the $1/s^{10}$ behavior of the fit can be viewed as the effective power behavior exhibited by $(s+m^2)^{-12}$ for the range of s ($s<45$ GeV^2) considered by Landshoff and Polkinghorne.[16] Note that unrestricted use of Eq. (13) implies that that $\alpha_{\text{eff}}(-\infty)=-0.5$ when, of course, $s\gg -t$.

The other special case with which we will be particularly concerned here is $\pi^- p$ scattering, corresponding to $B=D=2$, $A=C=1$ in the simplest model, in which the pion has a monopole form factor as expected in a two-quark model with no anomalous dimensions. Since $B=D+A-1$ the simple formula of Eq. (8) is logarithmically modified to

$$M\propto\frac{\ln(-t)}{(-t)^2}\frac{1}{u}\equiv F_p(t)\frac{1}{u}\,,$$

which is valid for arbitrary (asymptotic) t and u. Also, for $\pi^- p$ scattering there is in general a $(s\text{-}t)$ topology[17] interchange graph [Fig. 1(b)] which yields a contribution of the same form as above but with $u\longleftrightarrow s$. The relative size of these two contributions depends upon the quantum numbers carried by the constituents of the proton and pion. Inclusion of quark spin and a dimensional counting Born graph framework modify the above results slightly; for instance the $(u-t)$ topology alone yields $(d\sigma/dt)(\pi p\to\pi p)\propto 1/(t^4su^3)$.

We should also note that the form

$$N_B(x) \propto \theta\left(x - \tfrac{1}{2}\right)(1-x)^{n_B-1} + \theta\left(\tfrac{1}{2} - x\right)x^{n_B-1}, \quad (14)$$

with $n_B \equiv B$, while valid in either the $x \to 0$ or $x \to 1$ limit may be too simple for intermediate x values. In general there are other contributions to $N_B(x)$ of the same form but with $n_B > B$. This does not affect the $\pi^- p$ result [except to remove the $\ln(t)$] but would modify the pp result. In the latter case, for $u \gg t \gg m^2$, there is no longer a $1/u^B$, $1/u^2$ term arising from scaling x near 0 and the dominant contribution to M is

$$M \propto F_p(t)\frac{1}{u^3} \propto \frac{1}{t^2}\frac{1}{u^3}. \quad (15)$$

For arbitrary t and u this type of contribution is best approximated as

$$M \propto \frac{1}{su^2t^2} \quad (16)$$

in the case of pp scattering.

The above results may be reexpressed in terms of the behavior of effective trajectory and residue functions at asymptotic momentum transfer as follows. We are going to make an analysis using Regge theory at large angles where the criteria for the validity of the Regge expansion are not satisfied. However, the validity of the expansion used here depends only on how rapidly the Mandelstam double spectral functions approach their asymptotic form. This can occur even if the Regge criteria are not met. We define the spin-averaged differential cross section as

$$\frac{d\sigma}{dt} \propto \frac{1}{s^2}|M|^2$$

and take

$$M \propto (-u)^{\alpha(t)}\beta(t), \quad |u| \gg |t|$$
$$\propto (-t)^{\alpha(u)}\beta(u), \quad |t| \gg |u|.$$

For pp scattering we then have for the naive calculations described above,

$$\alpha(-\infty) = -2, \quad \beta(t) \propto \frac{1}{(-t)^3}, \quad (17)$$

though there are important, perhaps temporarily, dominant terms for which

$$\alpha(-\infty) = -3$$

and

$$\beta(t) \propto \frac{1}{(-t)^2}. \quad (18)$$

The more sophisticated three spin-$\frac{1}{2}$-quark model, with fixed-angle power behavior $d\sigma/dt \propto 1/s^{10}$ yields

$$\alpha(-\infty) = -1$$

and

$$\beta(t) \propto \frac{1}{(-t)^2}. \quad (19)$$

Even if the dipole behavior of the form factor and hence of the wave functions breaks down as $t \to -\infty$, the above α_{eff} predictions should be approximately correct over the sizeable kinematic regime for which the form factors exhibit dipole behavior. For πp scattering we obtain in the spinless case the asymptotic t-channel results for meson trajectories

$$\alpha_t(-\infty) = -1$$

and

$$\beta_t \propto \frac{1}{(-t)^2}, \quad (20)$$

while for the u-channel baryon trajectories,

$$\alpha_u(-\infty) = -2$$

and

$$\beta_u \propto \frac{1}{(-u)}. \quad (21)$$

In general, all of the above effective trajectory predictions hold for both the I = 0 and I = 1 t-channel trajectories and I = $\frac{1}{2}$ and $\frac{3}{2}$ u-channel trajectories.

The above πp scattering results are modified in the case of spin-$\frac{1}{2}$ quarks. One finds that $\alpha_{\text{eff}}(-\infty) = -\frac{3}{2}$ and $\beta_u \propto 1/(-u)^{3/2}$ in the backward direction (essentially because of the necessary helicity change in going from meson to nucleon) while the forward direction results are unchanged. The limiting values and forms given above depend sensitively on the detailed quark model assumed, especially on the angular distribution of quark-hadron elastic scattering. Dimensional-counting rules for $\alpha(-\infty)$ and $\beta(t)$ have been given in Ref. 3, Sec. V 4.

Unfortunately, currently available data cannot necessarily be said to be fully asymptotic in the above sense. Thus comparison of the interchange predictions to the effective trajectories and residues extracted (as described later) from the data, must proceed (particularly in the pp case) via performing exactly the same extraction procedure upon the full interchange expression—that is by treating the full theoretical result as data. These predicted trajectories should also hold in inclusive scattering where the increased data rate should allow the analysis to be extended to very large momentum transfers.

In addition one must not forget that an examination of the effects of higher-order iterated dia-

grams and of hadronic bremsstrahlung[8] indicates that interchange theory Reggeizes smoothly at small momentum transfers. Thus, even in a theory in which the interchange amplitude dominates at fixed angle for asymptotic energies, the leading trajectories may well be sufficiently high near $t \sim 0$ to produce the normal Regge intercepts while at large $(-t)$ joining smoothly on to the limiting values given above. Thus a direct extraction of the effective trajectories from experimental data will yield values which should decrease toward the above limiting values as $-t$ gets large. Secondly, it is quite clear that the effective trajectory behaves in an essentially different fashion in the pp and πp amplitudes. Consider pp scattering for a moment. At fixed s as t decreases from its value at 90° the iterated πp interchange process will begin to couple (see Fig. 3). Since $\alpha_{\rm eff}(\pi p) > \alpha_{\rm eff}(pp)$, it is clear that this effect will increase rapidly in importance as $-t$ decreases towards zero. It is only for quite large $-t$ that the effects of the higher-lying πp trajectory are very nearly canceled in pp scattering.[18] Thus as t decreases to moderate values the effective trajectory extracted for pp scattering should rise to the level of the higher-lying coupled πp trajectory. In contrast the πp effective trajectory (in the t channel) does not receive iterative contributions from any coupled channel with a still higher large t limit for its effective trajectory. In addition the πp effective trajectory limit is high to begin with. Thus, the complications due to coupled-channel iterative contributions are not likely to be phenomenologically significant except at relatively small t.

In cases where exotic trajectories are exchanged, such as backward $\bar{p}p$ (and $K^- p$) scattering, one might expect that the rise of the Regge trajectory as u decreases is small. Thus backward scattering should show a behavior characterized by $\alpha_{\bar{p}p}(u \sim 0) \sim \alpha_{\bar{p}p}(-\infty) = -4$, with a constant residue. Thus the backward cross section is predicted to behave as s^{-10}, which is consistent with the data even in the (exotic) backward peak region.

We turn now to the logarithmically trajectoried dual model (5) which can, for our purposes, be most transparently written as

$$
\begin{aligned}
&M = C(q) q^{\alpha(t)\alpha(u)} P\,, \\
&P = \sum_{n=0}^{\infty} \left(1 - \frac{q^n}{\tau\epsilon}\right)\left(1 - \frac{q^n}{\tau}\right)^{-1}\left(1 - \frac{q^n}{\epsilon}\right)^{-1} \\
&\quad = \frac{G(q/\tau\epsilon)}{G(q/\tau)G(q/\epsilon)}\,, \\
&\tau = b - at\,, \quad \epsilon = b - au\,, \\
&\alpha(t) = \frac{\ln\tau}{\ln q} = \alpha(t_0) + \frac{1}{\ln q}\ln\frac{1 - t/4M_q^{\,2}}{1 - t_0/4M_q^{\,2}}\,, \\
&\alpha(u) = \frac{\ln\epsilon}{\ln q}\,.
\end{aligned}
\tag{22}
$$

Note that the trajectory has a branch point at $4M_q^{\,2}$ which one might be tempted to identify with the threshold for "quark" production.[19]

It is apparent from the above equation that the parameter $1/\ln q$ plays the role of d of Eq. (5); in fact in the limit of large t and u the factor P of Eq. (22) becomes equal to unity and the dual amplitude reduces exactly to the form in Eq. (5). It has been argued[11] that for Coulomb scattering the Regge trajectories are logarithmic with the coefficient of the logarithm proportional to $g^2/4\pi$, the coupling of the vector gluon to the bound constituents. Then taking $g^2/4\pi \to 0$, in which limit one might expect to obtain an interchangelike amplitude (i.e., the diagrams of Fig. 2 vanish leaving those of Fig. 1), would be equivalent to $1/\ln q \to 0$, i.e., $q \to 0$ for the dual amplitude. It is apparent from Eq. (22) that if $\alpha(t_0)$ approaches a definite value α_0, as $q \to 0$, an interchangelike result obtains ($\alpha_0 < 0$ is required)

$$
M \sim C'(-t)^{\alpha_0}(-u)^{\alpha_0}\,. \tag{23}
$$

(This $u - t$–symmetric result is easily generalized.)

This proportionality between $1/\ln q$ and $g^2/4\pi$ is also suggested by the fact that the Veneziano amplitude is the $q \to 1$ limit of the more general amplitude of Eq. (22) provided that α',

$$
\alpha' = 1/4M_q^{\,2}\ln q\,, \tag{24}
$$

the slope of the resulting linear trajectory, is held fixed, and that $\alpha(t_0)$ approaches a definite limit. Physically this limit corresponds to large "quark" mass and large coupling constant. Infinitely massive quarks can only be bound to form finite massed hadronic states on an indefinitely rising linear trajectory if the coupling constant is infinite, again suggesting that

$$
\frac{g^2}{4\pi} \propto \frac{1}{\ln q}\,. \tag{25}
$$

If the "quark" mass were finite and the "quarks"

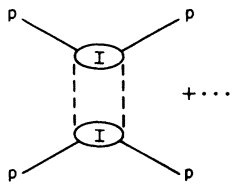

FIG. 3. Illustration of the coupling between $pp \to pp$ scattering and $p\pi \to p\pi$ scattering as t-channel iterations become important.

able to escape, there would exist at some energy an ionization point near which the trajectory would be very nonlinear.

Thus we see that there is a continuum of physically reasonable models with increasingly flat trajectories at large momentum transfer. Sufficient experimental information to distinguish between the dual models and the interchange model (with Reggeization complications included), in the case of pp scattering is not currently available. Similarly, a πp dual amplitude has not been developed theoretically. The difficulties in making this distinction will become apparent in the following sections. Among these models, the interchange model does have the advantage that results for other types of processes, meson and proton initiated processes as well as inclusive processes, are easily and unambiguously obtained (once form-factor behaviors are known or given) and appear to agree well with experimental data. It is not clear, however, that similar agreement cannot be obtained with the dual model. Higher-energy fixed-angle measurements (say for 60 GeV$^2 < s < 100$ GeV^2) together with correlated form-factor measurements would probably be definitive in the proton case, and are certainly highly desirable.

As a final note, we should, perhaps, emphasize one further complication which might be present and would make the distinction between interchange and dual models still more difficult. It is quite conceivable that form factors do not have fixed power law fall off at increasing momentum transfer, but rather the effective inverse power, n in $1/t^n$, could be an increasing function of $-t$. This is, in fact, expected in the above mentioned dual models, as well as in "scale-invariant" parton models.[20] Thus the wave function damping employed in the interchange computation should perhaps be a function of the kinematic range being examined.

III. DATA ANALYSIS

This section is devoted to an analysis of the existing data for pp and πp elastic scattering. Emphasis is given to the extraction of effective trajectory and residue functions at high momentum transfer. In performing this extraction it is essential to understand the variable dependence of the scattering amplitudes particularly when t is a substantial fraction of s. For large t the difference between s^α and u^α is substantial. For instance, if the amplitude actually was given exactly by

$$\beta(t)(-u)^{-n} \tag{26}$$

but the t-channel effective trajectory is extracted using the variable s, one would obtain

$$\alpha_{\text{eff}} = \frac{-n}{1 + t/s}, \tag{27}$$

by neglecting masses relative to t and s. That is, because of an inappropriate choice of variable, the extracted trajectory would be considerably lower than its ultimate value (for large $s \gg t$) if t is a resonable fraction of s. Correspondingly if one has data for more than one value of s at any given t, substantial variation in the extracted effective trajectory should be observed in this example.

These considerations are of crucial importance in the case of pp scattering. Most theories, including the dual models and the interchange theory, predict that the differential cross section should have the form

$$s(s - 4m^2)\frac{d\sigma}{dt} = (-u)^{2\alpha_{\text{eff}}(t)}|\beta(t)|^2 \quad (|u| \gg |t|). \tag{28}$$

That is, the invariant amplitude should reflect the underlying $(u - t)$ topology of the contributing diagrams. This requirement is equivalent to the requirement that the nondiffractive component of Regge behavior in pp scattering should be purely real, there being no direct channel resonance contributions. Thus as argued above power law behavior of the invariant amplitude will be more quickly revealed, and with less ambiguity, if effective trajectory and residue analyses are performed using the variables u and t.

A direct extraction of the effective trajectory from the data[21] according to Eq. (28) yields the results of Fig. 4. Figure 4(a) shows that the effective trajectory falls from 1 at small t in a nonlinear fashion to -2.7 at the largest t value for which the extraction can be performed. The pp data employed is that available with $s < 60$ GeV^2. There is now available data for $|t| < 10$ GeV^2 at ISR energies. As discussed in Sec. II, this region of s and t is dominated by the Pomeron cross-section contribution. The $\alpha_{\text{eff}}(t)$ extracted over the range $0 < |t| < 10$ GeV^2 is expected to make a transition to a relatively flat Pomeron-like trajectory, $\alpha_{\text{eff}}(t) \approx 1$, at ISR energies. For $s < 60$ GeV^2 this same t range is dominated by the non-Pomeron dual-interchange contributions on which we temporarily concentrate. The indicated errors on the $s < 60$ GeV^2 analysis arise mainly from a small s dependence of α_{eff} at any given t. [Usually α_{eff} tends to increase slightly as s increases at fixed t. In fact there is some evidence for a slight break in the s dependence at approximately $\ln(-u)$ for various integer t values.] The corresponding residue funciton is presented in Fig. 4(b). It is immediately apparent that the extracted residue tends to increase with increasing $-t$. This

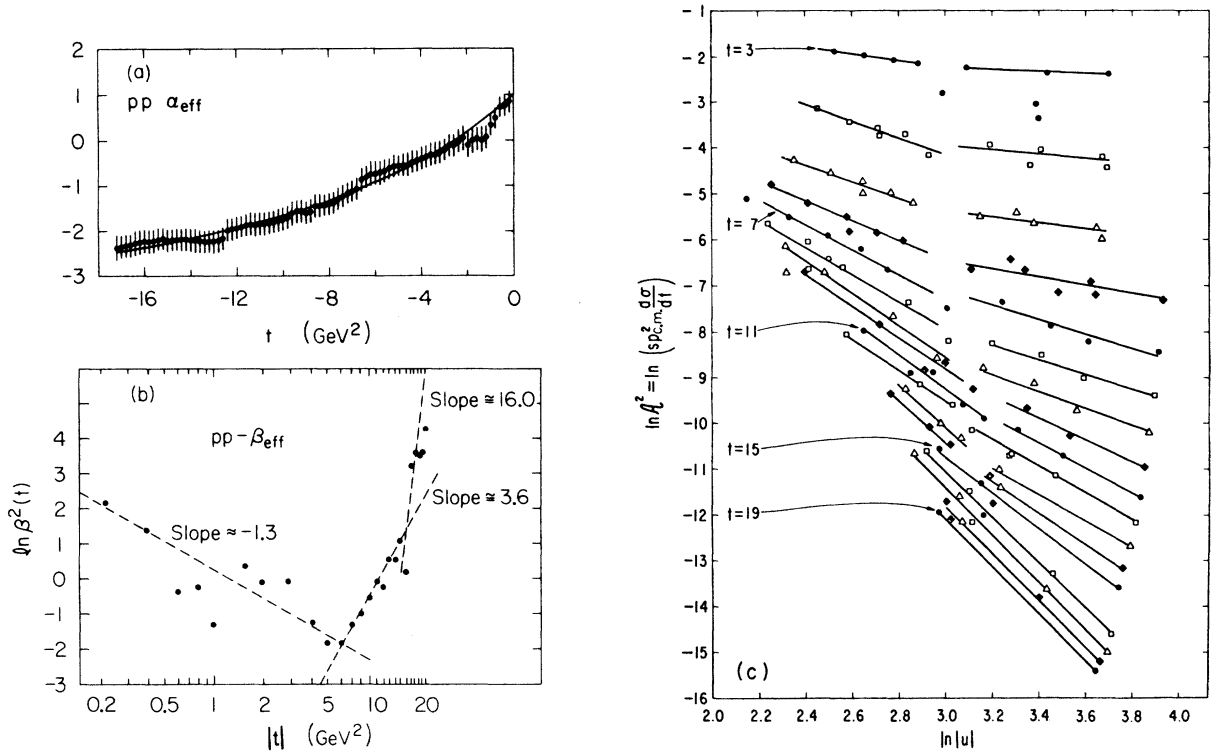

FIG. 4. (a) Extracted effective trajectory for pp elastic scattering. Error bars indicate typical amount of s dependence of extracted α_{eff} at any given t. The variable $(-u)$ is employed. (b) Extracted residue function, $\beta(t)$. (c) Plot of ln $[s^2(d\sigma/dt)]$ vs ln $(-u)$, indicating a possible change in slope (for given t value) as ln $(-u)$ increases.

behavior would seem in disagreement with the interchange predictions, for asymptotic Regge expressions, of Sec. I. However, from Eq. (11) we see that in the region of 90° ($z < 0.5$), secondary terms are significant and a more careful examination is required. We will return to this point in a moment.

First we give the results of the effective-trajectory extraction if the variable s is employed for the Regge dependence instead of the variable $-u$. These are given in Fig. 5. Two features of the graph are immediately apparent. First the effective trajectory falls much more rapidly in $-t$. Second, there is considerably more s dependence of the extracted trajectory at any given t (as indicated by the error bars[22]). In addition to which, a number of discontinuities appear which can be traced back to substantial changes in the s of the data corresponding to the t values on either side of the break. The above anomalies, we argue, are evidence in favor of the u-variable extraction being most meaningful.[23] However, regardless of which variable, u or s, is employed in the extraction it is important to note that α_{eff} and β_{eff}, considered as local functions of u (or s) and t

$$\left(\text{e.g.,}\quad 2\alpha_{eff}(u,t) = \frac{\partial \ln(s^2 d\sigma/dt)}{\partial \ln(-u)}\,,\right.$$

$$\left.\beta^2(u,t) = s^2\frac{d\sigma}{dt}/(-u)^{2\alpha_{eff}(u,t)}\right),$$

do provide a *unique* local characterization of the elastic-cross-section data and are capable of exposing, cleanly, certain cross-section trends which are less obvious in other types of analysis.

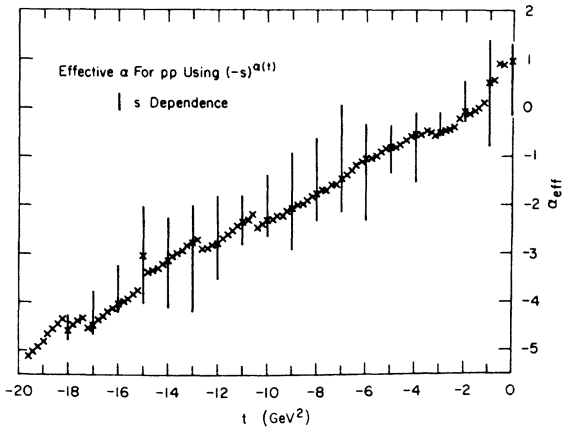

FIG. 5. Extracted effective trajectory using the variable s.

Thus, a comparison of α_{eff} and β_{eff} extracted from a given theoretical form with those extracted in identical fashion from experiment will reveal the extent to which the theory is a good representation of the cross section.

Let us return to assessing the degree to which interchange theory is able to describe the effective trajectory behavior given above. For this purpose we will take the form [see Eq. (12)]

$$\frac{d\sigma}{dt} \propto (s+m^2)^{-12}(1-z^2+4m^2/s)^{-6} \qquad (12')$$

as representative of the interchange result in the $s<60$ GeV^2 range. [Note in particular, that we use $1/s^{2n}(1-z^2)^n$, instead of the asymptotically equivalent form $1/(tu)^n$. Also, *ad hoc* mass corrections have been included.] We consider $t>3$ GeV^2 only, and take $m^2=1$ in Eq. (12a). Performing the α_{eff} extraction using Eq. (12a) evaluated at the kinematic points for which actual data is available, we obtain the results of Fig. 6. [Also given in this figure are the corresponding results for the Landshoff-Polkinghorne formula Eq. (13).] Two correlated differences between these graphs and those of Fig. 4 are immediately apparent. The effective trajectory of the interchange result is much flatter (for $t>3$ GeV^2) and the residue function, while not falling very rapidly, certainly

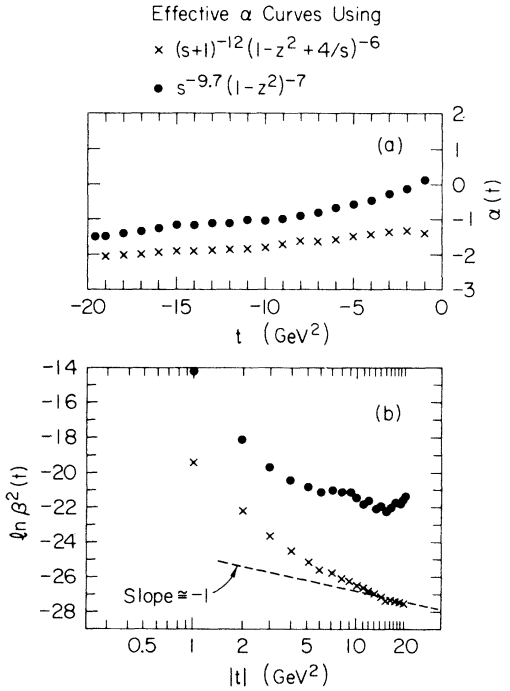

FIG. 6. (a) Effective-trajectory extractions performed using the theoretical cross-section forms of Eq. (12a) (interchange model) and Eq. (13). (b) Extracted residue functions corresponding to the above trajectories.

does not increase as for the actual data [t-channel Reggeization of the interchange graph can be expected, as discussed earlier, to lead to a much more steeply falling trajectory than the basic interchange graph alone; if the natural scale factor of the Reggeization, i.e., in $(-u/u_0)^{\alpha(t)}$, is then larger than 1, the residue discussed here will inevitably increase as $(-t)$ increases].

The above type of difference is, in a certain sense, second order. In the physical amplitude the decrease associated with a falling trajectory is compensated by the rising residue in such a way that an effectively flat trajectory with roughly constant residue gives approximately the same differential cross section in the kinematic range considered. In fact, if we restrict ourselves to $t/s>0.2$, the ratio of the experimental cross section to the theoretical cross section, Eq. (12a), does not change by much more than 50% from its central value for $s<60$ GeV^2 and in the range $20<s<40$ GeV^2 by no more than 30%. However, closer analysis as done here reveals definite systematic, and, as described earlier, expected differences, associated with the effects of Reggeization. These differences can best be summarized by the graph of Fig. 7 in which we schematically plot the logarithm of the differential cross section associated with a slowly-falling trajectory and constant residue function, in comparison to that associated with a more rapidly-falling trajectory and rising residue. The t range is chosen such that the fixed angular range coincides more or less with that of the actual data.

One sees that, for the lowest s value, over the given angular range the true cross section divided by the theoretical cross section (with flat residue, as indicated by the s independent intercept) should tend to increase as t increases, while just the opposite effect should be observed at high s. Careful numerical examination of the above ratio reveals such a trend. The point of crossover is in the vicinity of $s=35$ GeV^2. Examination of the above ratio is also useful in evaluating the relative merits of the $1/s^{10}$ behavior of Eq. (13), the Landshoff-Polkinghorne form. Use of this energy behavior introduces systematic discrepancies at the highest s values ($45<s<60$ GeV^2). To demonstrate this we have plotted in Fig. 8 the range of variation of the experimental-to-theoretical cross-section ratio (in arbitrary units) as a function of t for the various s values at which large-angle data is available. In Fig. 8(a), Eq. (12a) is compared to the experimental data (we require $t/s>0.2$ for this case) while in Fig. 8(b) we employ the Landshoff-Polkinghorne form Eq. (13) (we require $t/s>0.1$). For $s<40$ GeV^2, Eq. (13) works as well as Eq. (12a) did over the smaller t/s range,

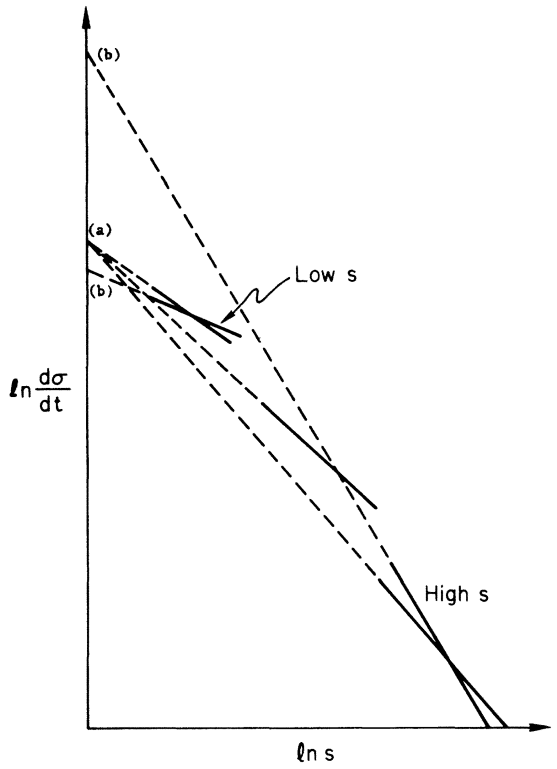

FIG. 7. Rough comparison of cross sections for which (a) the residue function (i.e., intercept on a log-log plot) is constant while the trajectory falls slowly (with increasing $-t$); and (b) the residue function grows as $-t$ increases but the trajectory falls more rapidly in such a way as to *approximately* compensate. The solid portions of the various lines indicate where in ln s the cross section is "measured". These "measurements" are extrapolated back to ln$s = 0$ to yield either (a), constant residue, or (b), a residue which grows with ln$s$ and correspondingly ln $|t|$. The respective curves are appropriately labeled. We have chosen the intermediate-energy curve to be common to the two cases. Note that the solid-line "measurements" always have a point of overlap.

except for the appearance of a systematic s dependence. (The ratio falls at high s indicating that the $1/s^{10}$ power is too weak). The improved t/s range of Eq. (13) is associated with its stronger z dependence. Were we to modify Eq. (12a) by increasing the power of the angle-dependent factor from 6 to 7, as might be appropriate after spin effects are included (the $\mathcal{P}\mathcal{N}$ quark pair probably have spin 1 in any realistic model), the t/s range over which 50% or less variation occurs is extended to $t/s > 0.1$. However, we see no reason to expect that fixed-angle formulas should work for $z > 0.6$ at present energies, in any case. [For either choice of z dependence in Eq. (12a) the systematic s dependence observed for Eq. (13) is considerably reduced.]

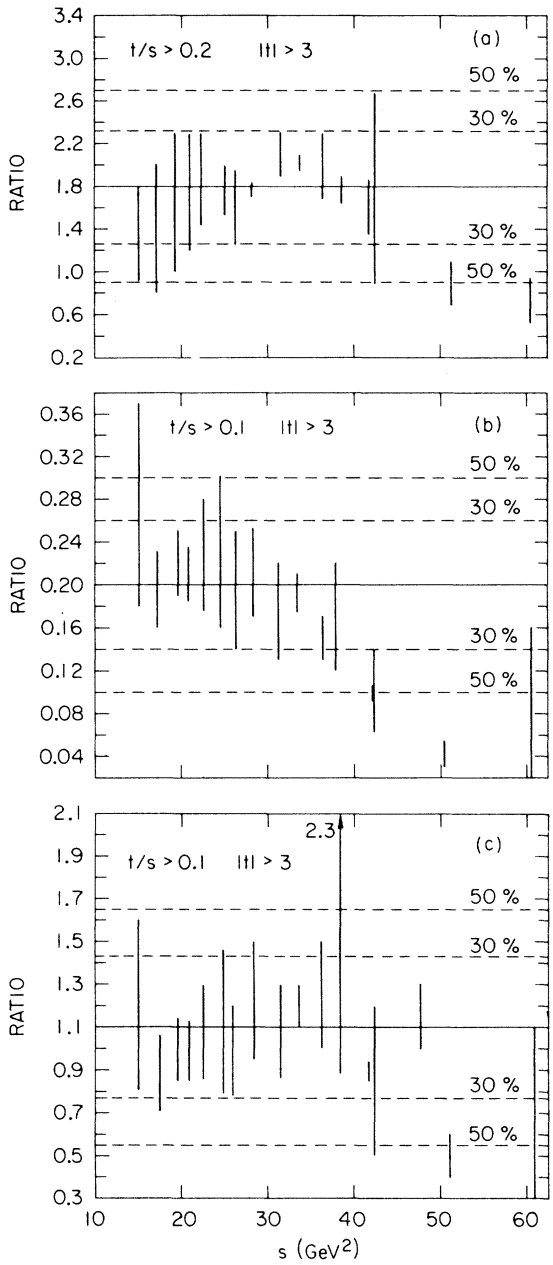

FIG. 8. Plots of the ratio of experimental cross section to theoretical cross section as a function of t for (a) Eq. (12a) (b) Eq. (13) (c) Eq. (12a), modified to have increased $(1-z^2)$ dependence, $1/(1-z^2)^7$.

The failure of a $1/s^{10}$ behavior, because of the fixed-angle nature of the data, is roughly equivalent to the observation that the Landshoff-Polkinghorne form, Eq. (13), will never yield an effective trajectory as low as the value -2.7 obtained at $t = -19$ GeV$/c^2$, even temporarily. [Recall that $\alpha_{\text{eff}} \to -0.5$ according to Eq. (13) when $s \gg t$.] Equation (12a) does considerably better in this regard.

For instance, at $t=-19$ Eq. (12a) gives $\alpha_{\text{eff}}=-2.1$ while Eq. (13) gives $\alpha_{\text{eff}}=-1.5$. Only for the modified N_B form, however, of Eq. (5) with $\alpha_{\text{eff}}=-3$ could the present trend of the extracted trajectory be said to be indicative of the eventual result. Of course, there exists the possibility mentioned at the end of Sec. I, that the wave functions employed in the interchange calculation should be given stronger damping than dipole, when probed in the $s>40$ GeV^2 kinematic range, in which case α_{eff} falls below -2. Direct measurements of the proton's electromagnetic form factor beyond $t=-25$ GeV^2 would determine whether such modification is necessary.

One should also keep in mind the possibility that while the $1/s^{12}$ behavior, corresponding to pn quark pairing within the proton, may be dominant at present energies, a $1/s^{10}$ behavior in which the pair is broken apart will, if present at all, ultimately dominate.

Finally we should note that if instead of $1/s^{2n}(1-z^2)^n$ in Eq. (12a) we used the asymptotically equivalent form $1/(tu)^n$ the results would have been significantly different, the latter form not being as consistent with the experimental data. This again illustrates the significance of mass corrections when $s<60$ GeV^2. Given this fact, the uncertainty in the form of the interchange formula itself and the complications of iterative Reggeization which are certain (particularly for pp scattering) to convert a fixed-angle formula such as Eq. (12a) into one with a rising trajectory (as $-t$ decreases in the present range, $-t<20$ GeV^2) it is difficult to decide whether or not an interchange description will work with precision for pp scattering at fixed angle. Only higher-s measurements will provide a definitive test.

The logarithmic-trajectory dual model provides a better description of the effective trajectory and residue. Though the full dual amplitude with no asymptotic approximations can be compared directly with the data, as is done in the next section, it is useful to examine an illustrative rough description of the data in which we drop all nonleading asymptotic terms. The large t and u limit of the dual amplitude is exactly given by Eq. (3) with d not equal to zero. That is the trajectory continues to fall as $-t$ increases in magnitude. More precisely from Eq. (22) we obtain

$$M\propto q^{\alpha(u)\,\alpha(t)}=(-u)^{\alpha(t)}(b-at)^{\ln b/\ln q}$$

with a logarithmically falling trajectory

$$\alpha(t)=\frac{\ln(b-at)}{\ln q},$$

i.e., M is completely determined by the three parameters a, b, and q which characterize the trajectory. We can determine the appropriate values for these parameters as follows:

(a) trajectory intercept $=\frac{1}{2}$ implies that

$$\frac{1}{2}=\frac{\ln b}{\ln q}\quad\text{or}\quad b=q^{1/2},$$

(b) the passing of the experimental trajectory through 0 at $t=-2$ GeV^2 implies

$$b+2a=1,$$

(c) the trajectory curvature determines q

$$q=\Delta t/\Delta t',$$

where Δt and $\Delta t'$ correspond to the t intervals between two successive changes of the trajectory α by one unit. From (c) and Fig. 4(a) we obtain $q=0.75$ which yields $b=0.86$, $a=0.07$. We should then have, roughly, at large t,

$$M\propto(-u)^{\alpha(t)}(-t)^{\ln b/\ln q}.$$

In this formula $\alpha(t)$, of course, fits the experimentally determined α_{eff} of Fig. 4(a) very well. From Fig. 4(b) we see that the experimental residue increases roughly only as t^2 though at the highest t values an increase of t^8 would not be inconsistent. However, this apparent disagreement for *moderate* t is purely an artifact of our asymptotic approximation which is not justified there. The small value of a [which from Eq. (28) is equivalent to a large Regge scale factor, $u_0=1/a$] implies that for the t and u range of present data the approximation $P=1$ is not valid. Even for very large u, where $G(q/\tau)$, $G(q/\epsilon)\sim 1$, we should, for moderate t, still include $1/G(q/\tau)$ in the residue function. The decrease of $1/G$ towards its large $(-t)$ limit of unity diminishes the rise of the effective residue function.

Thus in the dual model the parameters of the trajectory determine the residue function except for an overall constant. For a trajectory of the observed shape, the dual-model residue function is predicted to rise as $-t$ increases. This rise is simply due to the fact that the natural Regge scale factor (u_0) of the model is bigger than the 1-GeV scale factor used in the residue extraction. [Note that $(1/s_0)^\alpha$ increases as $-t$ increases if α decreases.] Thus the dual model provides a simple explanation of the rising extracted residue function. However, good agreement with experiment requires use of the full dual-model amplitude, which includes unambiguous nonasymptotic terms in P of Eq. (22) (associated with daughter trajectories). The most direct check of the ability of the dual model to describe the data is to attempt to fit the experimental data with the full amplitude. For this reason we leave detailed discussion of this case to the next section in which we will discuss

more detailed fits to the full angular range of pp elastic scattering which incorporate a Pomeron type of contribution in addition to the interchange- or dual-model amplitudes.

In the remainder of this section we turn to a discussion of πp elastic scattering for which interchange theory gives a fairly definite prediction, Eq. (20), which should not be strongly modified by effects of Reggeization except for quite small $-t$. We have extracted the effective trajectory in this case keeping in mind the fact that both (ut) and (st) graph topologies are in general present. This complicates the matrix element which must be used. Interchange theory predicts for πp scattering a large $(-t)$ cross section of the form

$$sp_{\text{c.m.}}^{\,2}\frac{d\sigma}{dt}=\beta^2(t)\,|2(-s)^{\alpha_{\text{eff}}(t)}+(-u)^{\alpha_{\text{eff}}(t)}|^2, \quad (29)$$

where $\alpha_{\text{eff}}\to -1$ as $t\to-\infty$. The relative magnitude of the two terms is fixed by simple quark-counting rules. Determination of the effective trajectory proceeds iteratively. First, a value for the α_{eff} associated with the second term is guessed and the data are then used to determine α_{eff} for the first term. The process is iterated until the two agree (as they must in any theory due to the relation of the two topologies by s-u crossing). The data of Ref. 24 for $\pi^- p$ were used and yield the effective trajectory and residue given in Figs. 9(a), 9(b). The trajectory values oscillate around $\alpha\sim -1$ for $(-t)>3$ GeV/c^2, as predicted by the interchange theory and in agreement with the values obtained by Owen *et al.*[24] in an analysis of their own data. One should note that this description of the data demands that both the $I=0$ and $I=1$ trajectories have the same limiting value. It is satisfying that the residue behavior exhibited in Fig. 9(b) is in accord with interchange expectations. The best power law fit to the residue function, corresponding to $\beta\propto 1/t^2$, is adequate over a substantial range of t.

Interestingly, the πp trajectory shows no indication of continuing to fall as $-t$ increases.[25] Such a fall would most probably be expected were a logarithmic dual model applicable. In πp scattering, the kinematic range for which α is observed to reach its relatively high asymptotic value is quite accessible, making this an important test of interchange theory for exclusive processes. It should be noted that the $\alpha_{\text{eff}}=-1$ limit depends only upon the behavior of the pion's wave function, an object predicted to have simple monopole behavior for arbitrarily large off-shell masses by the two-quark model. In addition this monopole behavior has been indirectly verified by the success of the interchange theory of high transverse momentum production of pions at the ISR.[26] The

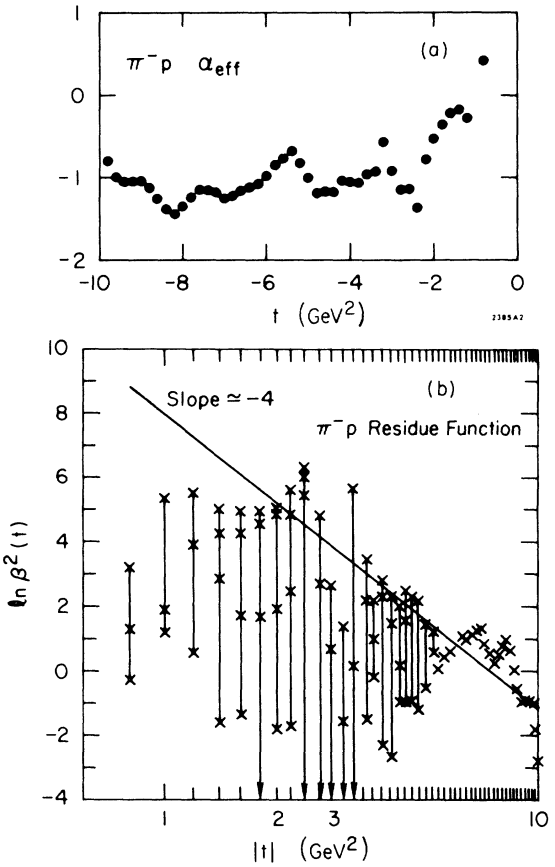

FIG. 9. (a) Effective trajectory for $\pi^- p$ elastic scattering, extracted using Eq. (29). (b) Corresponding residue function. As before error bars indicate s dependence of extracted values: t and $|t|$ in GeV^2.

above simplicity should apply also to processes such as photoproduction of pions for which interchange theory predicts a high $\alpha_{\text{eff}}(-\infty)$, as high, perhaps, as $-\frac{1}{2}$. [See Ref. 3 in which inclusive evidence for high α_{eff}'s in $\gamma+p\to(K,p,\pi)+X$ is discussed.]

Thus we have seen that effective trajectory analyses can provide a sensitive and useful means for describing data and pinpointing the nature of any proposed theoretical description of the data. The fit of Landshoff and Polkinghorne[15] to deep-elastic pp scattering, which is quite good on the average, is revealed as systematically different from the data. Inclusion of Reggeization effects in interchange models is necessary to describe the existing pp data with $s<50$ GeV^2. Higher-energy measurements will be required before any firm conclusion can be drawn concerning the validity of interchangelike formulas at fixed angle. It does appear, however, that forms with ultimate $1/s^{10}$ behavior are in trouble. In contrast, πp scattering with its relatively high asymptotic ef-

fective trajectory (resulting in the relative unimportance of Reggeization effects except at quite small $-t$) appears to be well described by the interchange result. A combination of Regge and CIM terms has been used to fit $\bar{p}p \to \pi^+\pi^-$ by Donnachie and Thomas.[25]

IV. PROTON-PROTON ELASTIC SCATTERING

This section attempts more complete phenomenological analyses of pp elastic scattering, based upon the interchange and dual models. Both models must be supplemented by a specific ansatz for the forward diffractive contribution. This forward diffractive contribution becomes more and more important as s increases at fixed t relative to the interchange- or dual-model contributions which dominate at lower s over much of the t range. In fact the effective-trajectory results presented in Figs. 4 and 5 do not include the ISR data[27,28] with $|t| \lesssim 10$ GeV^2. Were this data to be included α_{eff} would show a marked s dependence rising to near 1 at the ISR energies over this t range. At ISR energies much larger values of t are required before the interchange- or dual-model contributions can be expected to dominate—they are most important over a domain fixed in angle, not in t. In fact in the phenomonological analyses we demonstrate that by considering the cross section as a sum,

$$\frac{d\sigma}{dt} = \frac{d\sigma}{dt}^{\text{pomeron}} + \frac{d\sigma}{dt}^{\text{dual or interchange}},$$

one may use low energy $s < 60$ GeV^2 data plus the well determined dual-model or interchange forms to extract a Pomeron term which is in reasonably good agreement with the ISR results[27] for $|t| < 3$ GeV^2 where the Pomeron dominates, see Figs. 13 and 16. The Pomeron forms we employ are less satisfactory[29] in comparison to the latest ISR data with $3 < |t| < 10$ GeV^2 but the general pattern is clear. Any fixed-t value (greater than some typical mass^2) will be part of the fixed-angle regime at low enough s and the cross section described by $d\sigma/dt^{\text{dual or interchange}}$. At high enough s the dual or interchange contribution will have fallen away, exposing the roughly s-independent Pomeron contribution. This process has taken place for $|t| < 10$ GeV^2 by ISR energies, $\sqrt{s} \sim 50$ GeV.

A. Interchange theory

We will employ here the form of Eq. (28a) ignoring iterative Reggeization effects. Our aim here is not an absolutely precise fit to the large-angle region, but rather an attempt to use our relatively good understanding of this region as a tool in extracting from the data with $s < 45$ GeV^2 (the Coconni data is not included) the true shape of the Pomeron contribution. We find that the Pomeron must have substantial structure such as that of the form

$$P = isAe^{t(a+b\ln s)} + Cs\left(\frac{s}{s(p_L = 19.3\ \text{GeV}/c)}\right)^p (R\sqrt{-t}) J_1(R\sqrt{-t}) e^{ht}, \tag{30}$$

The first term is, of course, the normal forward peak with possible shrinkage allowed for (we restrict ourselves to $t > 0.1$ GeV$/c^2$). The second term can be thought of as an edge effect as suggested by Kane[30] and provides, as it turns out, the necessary structure, in the form of a sharp break, in the forward direction around $-t \sim 1.2$ GeV$/c^2$. In addition, this second term does have an important effect at high s values, out to $-t \sim 8$ and provides much of the extra contribution required in the $t/s < 0.2$ range where Eq. (28a), alone, predicts too small a cross section. The constant C is real for a true edge effect. The second term is required to vanish in the forward direction for simplicity. An equally good description of the data is possible in which this term is made pure imaginary, corresponding to a secondary diffractive minima or multi-Pomeron effect in which case the energy-dependent factor $[s/s(p_L = 19.3\ \text{GeV}/c)]$ should be replaced by some power of $\ln s$. The resulting "Pomeron" then has a very sharp dip such as that seen at ISR.

The best fit (28) to the data yields the values

$$\begin{aligned} &A = (70.0\ \mu\text{b})^{1/2}, \\ &a = 2.32, \quad b = 0.57, \\ &C = -0.594\ [\mu\text{b}/(\text{GeV}/c)]^{1/2}, \\ &p = -0.335, \quad R = 0.784, \quad h = 1.14, \end{aligned} \tag{31}$$

where the parameters are given in GeV$/c$ units.

The interchange contribution will include the inevitable and very necessary mass corrections of Eq. (12a) in a slightly more general form. These corrections are present, of course, in any nonasymptotic description of the form factors. These not only render it finite at $z = 1$ but they also tend to increase the level of the effective trajectory for the interchange contribution at small $-t$. This latter trend is desirable as we know from Sec. II. Assuming that the nucleon form factors ultimately fall as dipoles, the interchange amplitude will be written as[31]

$$I = N(1 - z^2 + 4m^2/s)^{-3}(s + 4\lambda^2)^{-6}, \tag{32}$$

which yields Eq. (13) in the asymptotic limit. The total scattering amplitude is then $P + I$. The fit

could be improved by slightly increasing the assumed fall off of the form factors but this will not be done here. The best values of the parameters in I are all reasonable and turn out to be

$$m^2 = 1.06, \quad \lambda^2 = 0.784,$$
$$N = 1.42 \times 10^{-7}[s(p_L = 19.3 \text{ GeV}/c)]^6 \ (\mu\text{b})^{1/2}. \tag{33}$$

The above amplitude is compared with the data in Fig. 10. The χ^2 of the fit was 646 for 395 data points; nine parameters were adjusted.

A number of qualitative features of this description of pp elastic scattering are of particular interest. One may isolate the contributions to the amplitude of the three terms, for various values of the energy. A physical picture immediately emerges. For low values of laboratory momentum, the interchange contribution I hides the secondary "hump" structure of the Pomeron. However, since I falls rapidly with the energy, the secondary maximum becomes increasingly exposed as p_{lab} increases. Indeed at ISR energies, the interchange contribution is exceedingly small for the moderate $-t$ values (< 6 GeV^2) measured so far. Thus the ISR data reflects only the forward diffractive effects. It is interesting to note that the extrapolation of our diffractive terms (with parameters determined from the intermediate energy data) to ISR energies is in good qualitative agreement with the data. Thus the interchange description of fixed-angle scattering has allowed us to account reasonably successfully for the non-Pomeron portion of the scattering amplitude making even a moderate energy extraction of the purely diffractive terms, including otherwise hidden structure, possible.

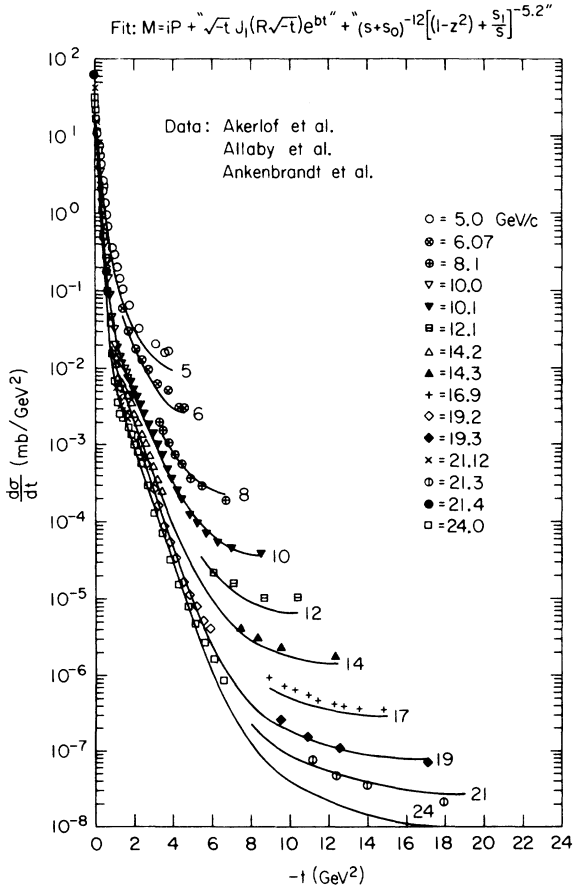

FIG. 10. Comparison of the phenomenological cross section for the interchange fit [Eqs. (30), (31), (32), (33)] to the pp elastic scattering data.

Thus, in elastic pp scattering we may be seeing relatively clearly the two most basic types of interaction mechanisms likely to occur on the parton, i.e., proton constituent, level. It has been shown that the ISR Pomeron shape for $|t| < 3$ GeV^2 (which is much like that at lower energies according to the above extraction) is well described in a sophisticated version of the Chou-Yang model[32] which in its simplest form says

$$\frac{d\sigma}{dt} = G^4(t) \tag{34}$$

as a result of the contribution of diagrams such as that of Fig. 11, i.e., vector-gluon exchange between the partons. [The more sophisticated versions of this model include s-channel iterative effects which cause the Pomeron to have substantial structure and to be smaller at large t relative to its $t = 0$ value than in the simpler model of Eq. (34).] The large t region is reasonably well described by the other fundamental interaction, parton interchange. This contribution as we have seen, can also be important at small t and moderate s for which it obscures the Pomeron structure. As s increases more and more of the first contribution is uncovered.

B. Dual model

A glance at the pp elastic scattering data of Fig. 12 shows that there is a strongly energy-dependent

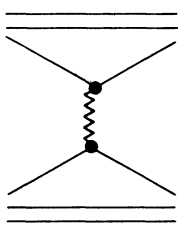

FIG. 11. Vector-gluon-exchange contribution to proton-proton elastic scattering.

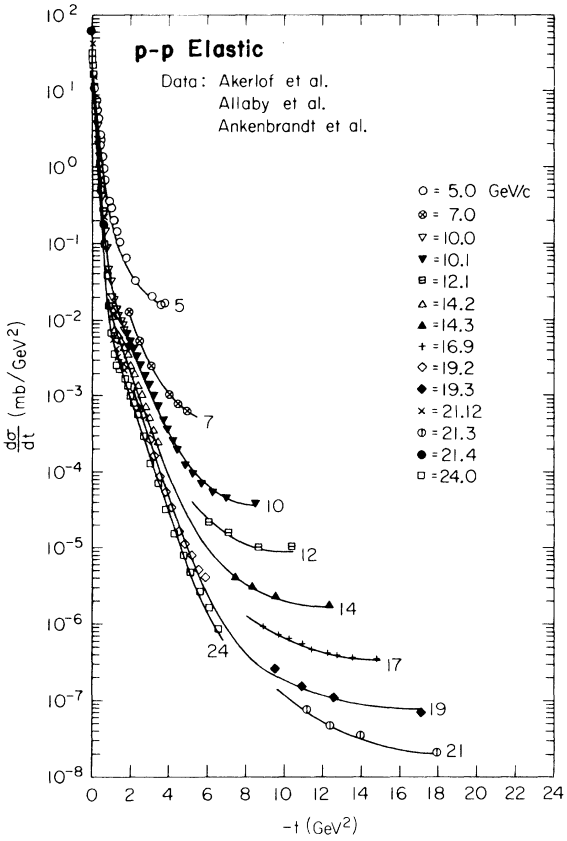

FIG. 12. Comparison of theoretical curves with high-energy pp elastic scattering data.

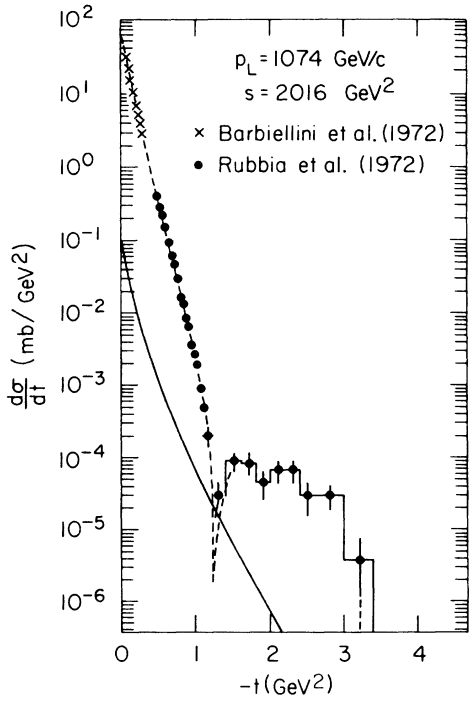

FIG. 13. pp data at ISR energy $s = 2016$ GeV^2. The dual contribution (solid line) passes just below the dip at $t \simeq -1.3$ GeV^2. Subtraction of the dual contribution from the experimental data Eq. (4) yields the dashed "pure" Pomeron curve.

contribution associated with the positive curvature "tails" in the $\ln(d\sigma/dt)$ plots. This positive-curvature contribution is smaller at higher energies and at sufficiently high energy an energy-independent diffraction minimum is revealed, Fig. 13, at $t = -1.3$ GeV^2 followed by a maximum at $t = -2$ GeV^2. The energy-independent diffractive component has negative curvature and its effects are easily recognized at moderate energies. The philosophy of the dual-model fit is to identify these two contributions with normal Regge terms and the Pomeron in accordance with the Harari-Freund hypothesis.[33] The only new feature is the range of t over which the Regge ideas are applied. The dual-model fit of Ref. 6 works very well out to $t = -24$ GeV^2. In fact, one dual term provides a very good description of the data in the region $-t > 5$ GeV^2 and $s > 18$ GeV^2. As has been noted by Barger *et al.*[23] another Regge exchange contribution is needed in the region $s < 18$ GeV^2. This is in accord with our α_{eff} extraction and is related to our $p_{\text{lab}} > 8.5$ GeV/c cut in the data. The point is that there is a lower-lying trajectory falling off faster in $-t$ than the trajectory of Fig. 4. This trajectory has sufficient coupling strength to be important up to $s = 18$ GeV^2. Dual-model fits to the lower-energy range as well as the higher-energy range are fully in accord with this picture. That is, good fits are obtained with a sum of two dual terms, each involving different trajectories. Since the Pomeron contribution to 90°-scattering data is negligible we can use the 90°-data to demonstrate how the second trajectory contributes to the $s < 18$ GeV^2 region. In Fig. 14 we show curves for the one dual term (1) and two dual term (2) contributions to pp 90°-data. Note that the slight nonlinear behavior of the 90°-data is described with precision. Of course, from the 90°-data alone one could not infer the presence of two trajectories. However, since the dual-model fit covers a vast area of the s, t plane and there does appear to be more than one trajectory contributing in pp elastic scattering, linear fits to 90°-data may represent an oversimplification of the underlying dynamics. The parton-interchange model relates the near linearity of the 90°-curve to the near dipole behavior of the proton form factor and does not predict that the 90°-curve should be perfectly linear.

When dual-model fits to the $|t| > 5$ GeV^2 region are extrapolated back into the region where the Pomeron contribution is important, it is found that the dual component accounts for nearly all

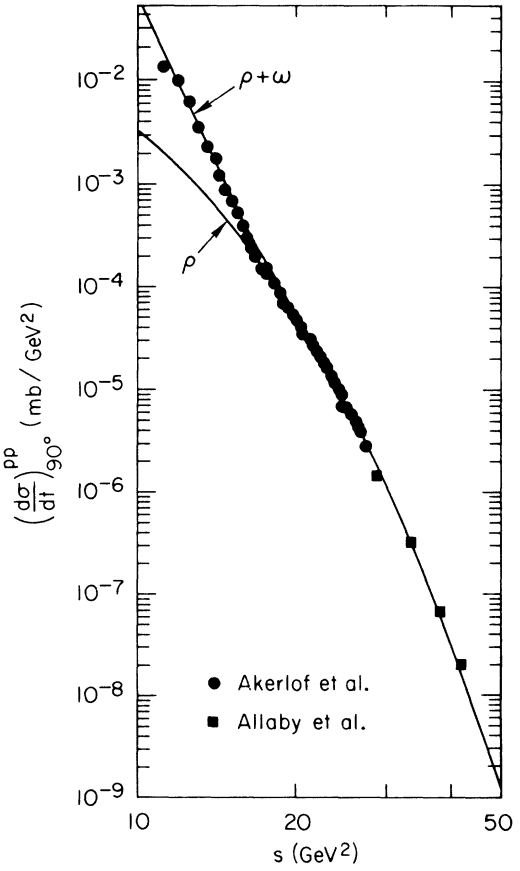

FIG. 14. Comparison of experimental points with theoretical dual-model curves for 90° pp scattering.

of the cross section at the $t=-1.3$ GeV^2 shoulder as in Fig. 15. Thus, the Pomeron component is seen to have a much sharper dip (dashed line in Fig. 15) than is visible in the data itself. Amazingly, when the dual contribution is extrapolated to ISR energies, it still appears to be contributing at the $t=-1.3$ GeV^2 dip (Fig. 13) and determining how much of the diffraction minimum is revealed. In Fig. 16 we show curves for an extracted Pomeron contribution assuming that the Pomeron is purely imaginary and using

$$\left(\frac{d\sigma}{dt}\right)_{\text{Pomeron}} = \left(\frac{d\sigma}{dt}\right)_{\text{experimental}} - \left(\frac{d\sigma}{dt}\right)_{\text{dual}} ;$$

Note that the dual contribution to pp scattering is purely real. It is remarkable that the extracted Pomeron contributions present the same qualitative features at low energies as at ISR energies:

dip structure at $t\simeq -1$, 3 GeV^2,

same slope for large t: $A=1$, 9 GeV^{-2}.

In order to obtain a fit at all angles[6] we add an eikonalized Chou-Yang[32] Pomeron-exchange term

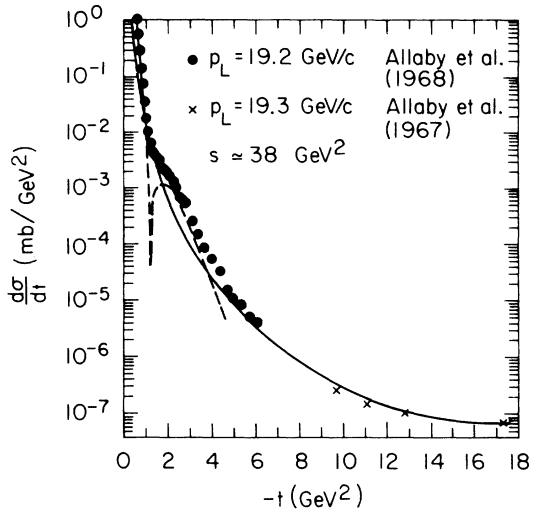

FIG. 15. Differential cross section for pp elastic scattering at $p_L \simeq 19.2$ GeV/c. The solid and dashed lines are the dual and "pure" Pomeron contributions, respectively.

to our two dual terms. Details are given in Ref. 6. The comparison with experimental data at moderate energies (12–24 GeV) is shown in Fig. 12. For ISR energies, especially for $|t|>2$ GeV^2,

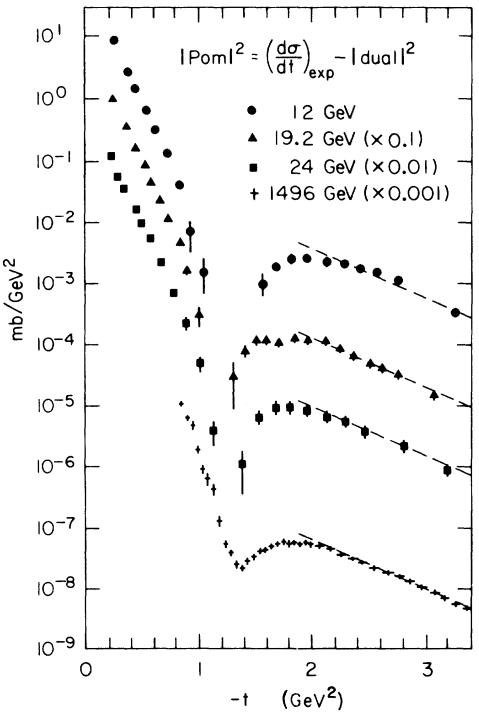

FIG. 16. Pomeron contributions at various energies obtianed by subtracting the dual (normal Reggeon) contribution. Note the dip structure around $t=1.3$ (GeV)^2 and the same slope for $|t|>2$ GeV^2 at all energies. The solid lines represent a falloff with a slope $A=1.9$ GeV^{-2}.

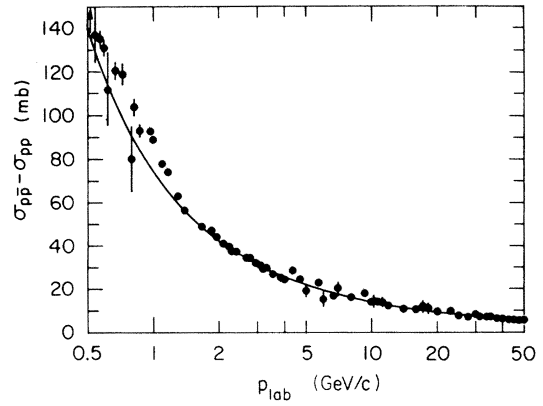

FIG. 17. The solid curve is the dual contribution to $\sigma_{tot}(\bar{p}p) - \sigma_{tot}(pp)$ and the points are values determined from experimental data.

Chou-Yang Pomeron-exchange term gives a too rapid fall off with t and inclusion of diffractive dissociation is necessary to describe the data.[29]

In addition to the differential cross section the dual model (with the zero-width resonances smoothed out[16]) together with the optical theorem was used to fit the $\bar{p}p/pp$ total-cross-section difference[6,7] and the ratio of real to imaginary part for pp scattering amplitude. (See Figs. 17 and 18.) We observe that $\sigma(\bar{p}p) - \sigma(pp)$ is well described for $p_{lab} > 1.3$ GeV/c and the ratio of the real to imaginary part works well for $p_{lab} > 4$ GeV/c. The two trajectories of the dual amplitudes were constrained to have the same q which was found to be $q = 0.795$. Their intercepts were $\alpha_1(0) = 0.8$ and $\alpha_2(0) = 0.37$ and the coupling of α_2 was found to be much greater than that of α_1. One might speculate that there is a connection between these two Regge contributions and the $\phi\omega\pi$ quark pairing or no pairing possibilities discussed in Sec. III. The coupling of the lower-lying effective parton-model trajectory (with pairing) is expected (and is found) to be greater than the higher-lying trajectory.

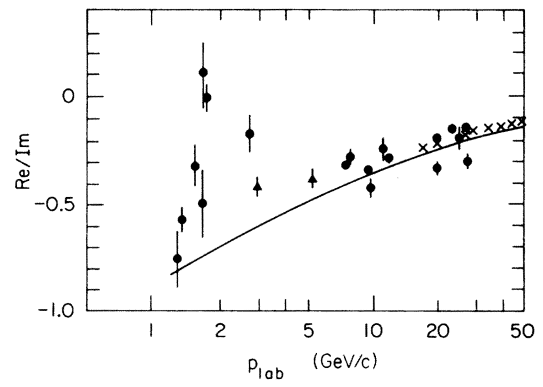

FIG. 18. The solid curve is the predicted ratio of the real to imaginary part of the forward pp amplitude. The imaginary part is computed from the proton-proton total cross section.

A different possibility was proposed in Ref. 6. There the trajectory with the weakest coupling, α_1, was identified with α_ρ and it was noted that Serpuhkov measurements of $\pi^+ p$ and $\pi^- p$ total cross sections give $\alpha_\rho = 0.7$ which is higher than the charge exchange value of $\alpha_\rho = 0.5$ and near the value of $\alpha_1(0) = 0.7$. The second trajectory which couples strongly was identified with the ω and the intercept $\alpha_2(0) = 0.37$ is just the conventional value of the ω intercept. With this identification, universality of ω and ρ couplings turns out to be approximately true in the range 5 GeV/$c < p_{lab} < 25$ GeV/c. For $p_{lab} = 12$ GeV/c and $t = 0$, the ratio of ω to ρ contributions was found to be 10 as compared with the expected theoretical value of 9 (Ref. 34).

Arik[7] has argued for a slightly different parametrization of α_2 and identified it with an exchange-degenerate ω, ρ, f, and A_2 trajectory. He takes $q = 0.9$ for α_2 so that the spectrum of leading meson recurrences is more linear and very close to the observed spectrum.

IV. CONCLUSIONS

In this paper we have attempted to make several points ranging from the theoretical to the phenomenological. In this latter category, it has been shown that attempts to extract effective trajectories at large momentum transfer from the presently available (finite-energy) data are model dependent. This effect arises from the difference between the two asymptotically equivalent Regge forms for the energy dependence of the amplitude, s^α or $(-u)^\alpha$. A model must be used to assign the proper linear combination of these forms. However, it was shown that in the case of pp scattering the theoretically preferable, s-channel exotic, (ut) form $(-u)^{\alpha(t)}$ of the amplitude gave a more energy-independent effective trajectory than the naive (st) form. Thus the data itself can be used to restrict the possible combinations if it is sufficiently accurate and copious.

The trajectories that were found here for pp and $\pi^- p$ scattering were not linear. They were much flatter at large momentum transfers than the conventional ones. Whether these trajectories ultimately approach negative constants (which must be integers if dimensional counting is correct) or fall slowly (such as in the logarithmic-trajectory dual model) cannot be answered with certainty at the present time. The $\pi^- p$ data seems to strongly prefer the flat trajectories of the interchange model at large $|t|$. This reaction also has

a trajectory shich is definitely higher than that found in the pp case. This situation could only occur if there is a cancellation of the leading trajectory in the pp case such as is found to be theoretically necessary to enforce factorization and the proper fixed-angle behavior.[10] One should always keep in mind that the effective trajectories are just that, and they are expected to vary with energy due to the contributions from cuts, subsidiary trajectories, etc. This may be especially important at small t, whereas the large t limits should be quite independent of s.

Both the CIM and the LDM agree well in a global sense with the pp data. However, the detailed agreement of the dual model is clearly superior. The effective Regge residue extracted from the data clearly reflects this fact, since the dual-model residue prediction is in better agreement with the data than is the CIM. An additional feature of both model fits is that the structure of the Pomeron which is required to fit the "shoulder" in the vicinity of $t \simeq -1.3$ GeV^2 at intermediate energies ($s \lesssim 60$ GeV^2) is in remarkable agreement with the structure observed at the CERN ISR in pp elastic scattering.

The overall result of our study of the large $|t|$ region for pp and $\pi^- p$ scattering is that there is strong phenomenological evidence that the forward and backward coherent Regge regions smoothly extrapolate to the same fixed-angle behavior in the central region ($\theta \sim 90°$). This extended duality is a strong restriction on the theory and provides rather unusual and unexpected connections between Regge trajectories and residues.

We have also found in this work that there may be a close relationship between the CIM and LDM and that the latter theory goes over into the former as certain coupling constants approach limiting values. It is already well known that there is a limit in which the LDM goes over into the ordinary dual model with linear trajectories.

The simple behavior of the data at large momentum transfers, and the simple interpretation given in theoretical terms by the CIM and the LDM should provide an interesting area of study. Clearly more data is required on more reactions at more energies at all angles before the validity of the theoretical ideas used here can be fully assessed. However, the agreement already established on a variety of reactions at energies which range from $p_{\text{lab}} \sim 5$ GeV/c to the ISR is impressive and encouraging.

ACKNOWLEDGMENT

This work was supported in part by the U. S. Department of Energy.

[1]J. F. Gunion, S. J. Brodsky, and R. Blankenbecler, Phys. Lett. 39B, 649 (1972) and Phys. Rev. D 8, 287 (1973) give the elastic predictions and theory.

[2]J. F. Gunion, S. J. Brodsky, and R. Blankenbecler, Phys. Rev. D 6, 2652 (1972) gives the basic inclusive results; Phys. Lett. 42B, 461 (1973) discusses the inclusion of bremsstrahlung and the application to $pp \to \pi$ at high transverse momentum.

[3]D. Sivers, S. J. Brodsky, and R. Blankenbecler, Phys. Rep. 23C, 1 (1976).

[4]P. V. Landshoff and J. C. Polkinghorne, Phys. Rev. D 8, 927 (1973) and J. C. Polkinghorne, in Proceedings of the Second International Conference on Elementary Particles, Aix-en-Provence, 1973 [J. Phys. (Paris) Suppl. 34, C 1-421 (1973)] have criticized and discussed the theory of Refs. 1, 2.

[5]M. Baker and D. D. Coon, Phys. Rev. D 13, 707 (1976) and 2, 2349 (1970) give the dual model theory.

[6]D. D. Coon, D. Sukhatme, and J. Trân Thanh Vân, Phys. Lett. B45, 287 (1973) gives pp elastic considerations. See also D. D. Coon and J. Trân Thanh Vân, in *The Pomeron*, proceedings of the VIII Rencontre de Moriond, Méribel-lès-Allues, France, 1973, edited by J. Trân Thanh Vân (CNRS, Paris, 1973).

[7]M. Arik, Phys. Rev. D 11, 602 (1975) gives additional phenomenological dual-model results.

[8]M. Arik, Phys. Rev. D 9, 3467 (1974).

[9]R. Blankenbecler and S. J. Brodsky, Phys. Rev. D 10, 2973 (1974).

[10]R. Blankenbecler, S. J. Brodsky, J. F. Gunion, and R. Savit, Phys. Rev. D 8, 4117 (1973); *ibid.* 10, 2153 (1974).

[11]D. D. Coon and H. Suura, Phys. Rev. D 10, 348 (1974).

[12]See I. Muzinich and P. Fishbane, BNL report, 1973 (unpublished) for possible complications, and M. Schmidt, Phys. Rev. D 9, 408 (1974) for possible solutions.

[13]This is what happened in the case of old-fashioned perturbation-theory wave functions.

[14]S. Brodsky and G. Farrar, Phys. Rev. Lett. 31, 1153 (1973); Phys. Rev. D 11, 1309 (1975).

[15]P. Landshoff and J. Polkinghorne, Phys. Rev. D 10, 891 (1974).

[16]The effective power of $1/(s+m^2)^{12}$ is $12/(1+m^2/s)$ which in the kinematic regime of $s < 60$ GeV^2 varies from 10 to 12, as s increases, for reasonable values of m^2.

[17]A third (su) topology also appears in the naive three-quark model of the proton. Compared to the ut and st topology contributions, $1/ut^2$and $1/st^2$, which is clearly suppressed in the t-channel Regge region $s \sim u \gg t$. Even at 90° it is suppressed by a factor of 4 in πp scattering. Only in the backward direction where it is comparable to the ut topology need it be included. This third topology which requires splitting apart the three quarks of the proton is absent in models of the proton with pn quark pairing.

[18]This cancellation is simply understood as a constraint imposed by the fact that the parton-interchange "Born term" controls the $t \to -\infty$ behavior of trajectories, in complete analogy with the situation in potential scattering.

[19]See M. Arik and D. D. Coon, Phys. Lett. 48B, 141 (1974).
[20]J. Kogut and L. Susskind, Phys. Rev. D 9, 697 (1974).
[21]The data are those of C. M. Ankenbrandt *et al.*, Phys. Rev. 170, 1223 (1968); J. V. Allaby, Phys. Lett. 23, 389 (1966); 25B, 156 (1967); 27B, 49 (1968); 288, 67 (1968); 34B, 431 (1971); C. W. Akerlof *et al.*, Phys. Rev. 159, 1198 (1957); G. Cocconi *et al.*, *ibid.* 138, 185 (1965). This last set of data with the highest s values is entirely responsible for the $s>45$ GeV^2 $t>15$ GeV^2 region of the trajectory extraction. Its large error bars have been ignored throughout the present section. We use only data with $p_{lab}>3.5$ GeV/c in the following analysis. The pp effective trajectory analyses do not include the latest ISR data with a moderately substantial t range. The effect this data would have is discussed in text.
[22]The s dependence was estimated by the following procedure: The experimentally available s values at any given t were ordered sequentially. The trajectory value appropriate to every neighboring pair was then computed. The highest and lowest values were discarded and the upper limit of the error bar computed as the average of the next two highest values, with a similar procedure for the lower limit.
[23]V. Barger, K. Geer, and F. Halzen, Nucl. Phys. B49, 302 (1972) do the s analysis over a more limited set of data. A very thorough analysis of the complete range of data is found in V. Barger, F. Halzen, and R. Phillips, Nucl. Phys. B61, 522 (1974).
[24]The πp data here are those of D. P. Owen *et al.*, Phys. Rev. 181, 1794 (1969); V. Chabaud *et al.*, Phys. Lett. 38B, 441 (1972); Carnillon *et al.*, Phys. Rev. Lett. 50, 403 (1973); R. Rubinstein *et al.*, *ibid.* 30, 1010 (1973). Insufficient π^+p data prevents a similar extraction in its case.
[25]An analysis of pion-nucleon charge exchange has also been carried out by R. Pearson (private communication). The leading effective trajectory in this case has the same general behavior as found above. See also W. S. Brockett *et al.*, Phys. Lett. 51B, 390 (1974); and A. Donnachie and P. R. Thomas, Nuovo Cimento 19A, 279 (1974).
[26]In fact, the inclusive data at 90° requires the monopole behavior to be valid for off-shell masses as high as 60 GeV^2. No indirect test of this sort exists for the proton wave function.
[27]H. De Kerrett *et al.*, Phys. Lett. 62B, 363 (1976).
[28]G. Barbiellini *et al.*, Phys. Lett. 39B, 663 (1972); A. Böhm *et al.*, *ibid.* 49B, 491 (1974).
[29]U. Sukhatme, Phys. Rev. Lett. 38, 124 (1977); and in *Leptons and Multileptons*, proceedings XII Rencontre de Moriond, edited by J. Trân Thanh Vân (Editions Frontières, Paris, 1977).
[30]G. Kane, Phys. Lett. 40B, 363 (1972).
[31]See Ref. 1 for details.
[32]T. T. Chou and C. N. Yang, Phys. Rev. 178, 1591 (1968); H. Moreno and R. Suaya, Report No. SLAC-PUB-1161, Stanford Linear Accelerator Center (unpublished); L. Durand, III and R. Lipes, Phys. Rev. Lett. 20, 637 (1968); S. C. Frautschi and B. Margolis, Nuovo Cimento 56A, 1155 (1968); J. Finkelstein, *ibid.* 59A, 92 (1969); A. Capella, J. Kaplan, A. Krzywicki, and D. Schiff, *ibid.* 63A, 141 (1969). See also C. Hojvat and J. Orear, Cornell Report No. CLNS-346 (unpublished).
[33]P. G. O. Freund, Phys. Rev. Lett. 20, 235 (1968); H. Harari, *ibid.* 20, 1395 (1968).
[34]See, for example, V. Barger and D. Cline, *Phenomenological Theories of High Energy Scattering* (Benjamin, New York, 1969).

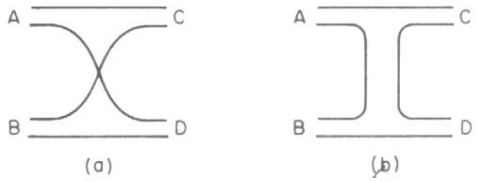

FIG. 1. (a) Interchange topology—*ut* diagram. (b) Interchange topology—*st* diagram.

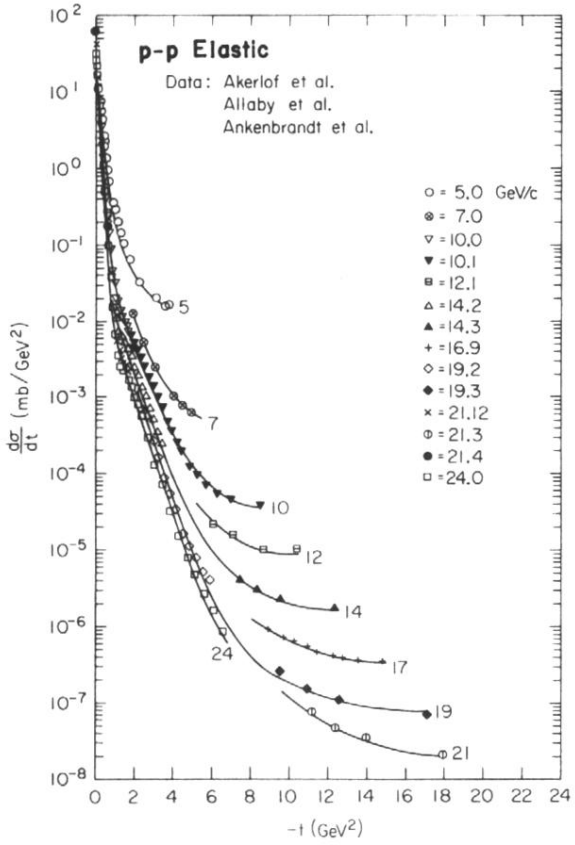

FIG. 12. Comparison of theoretical curves with high-energy pp elastic scattering data.

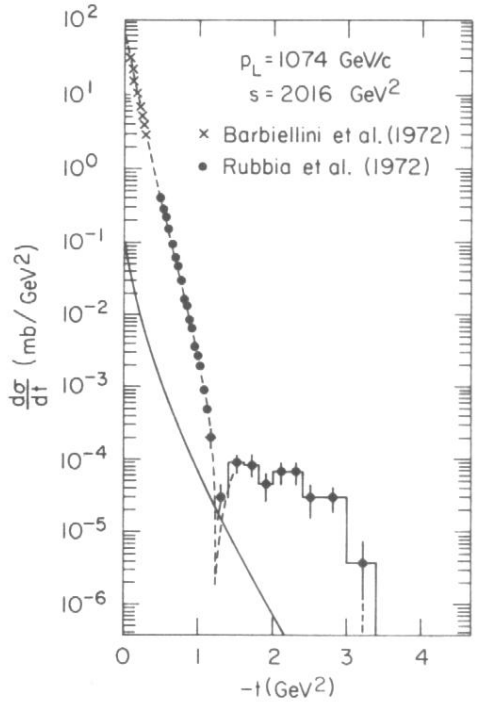

FIG. 13. pp data at ISR energy $s = 2016$ GeV^2. The dual contribution (solid line) passes just below the dip at $t \simeq -1.3$ GeV^2. Subtraction of the dual contribution from the experimental data Eq. (4) yields the dashed "pure" Pomeron curve.

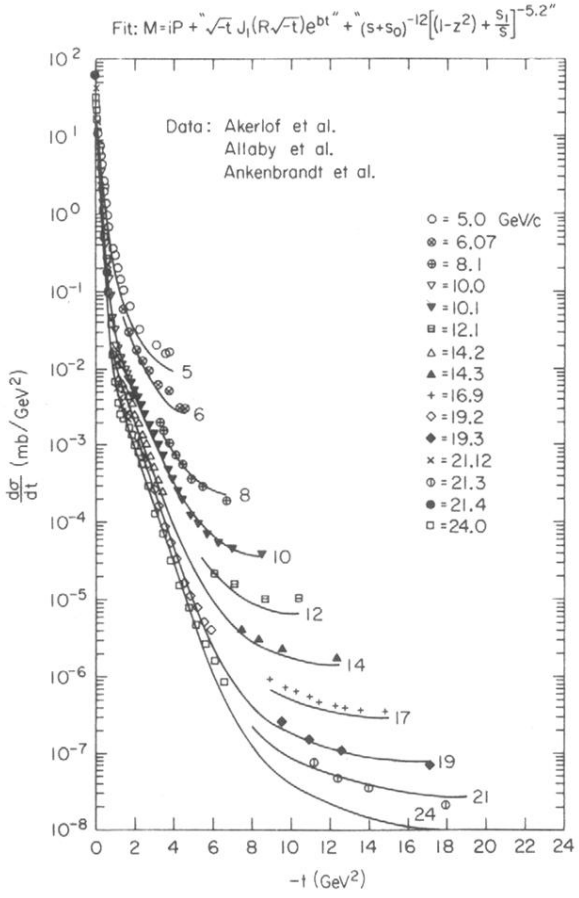

FIG. 10. Comparison of the phenomenological cross section for the interchange fit [Eqs. (30), (31), (32), (33)] to the *pp* elastic scattering data.

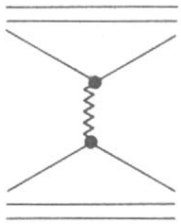

FIG. 11. Vector-gluon-exchange contribution to proton-proton elastic scattering.

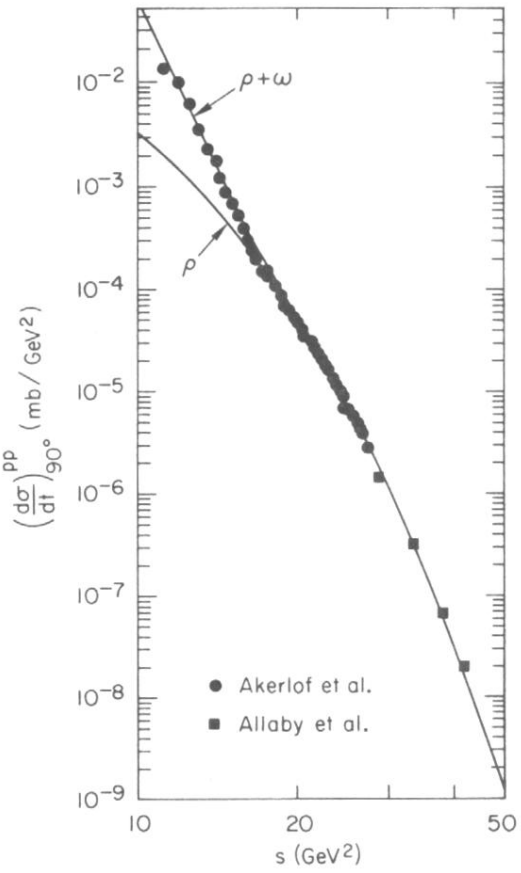

FIG. 14. Comparison of experimental points with theoretical dual-model curves for 90° pp scattering.

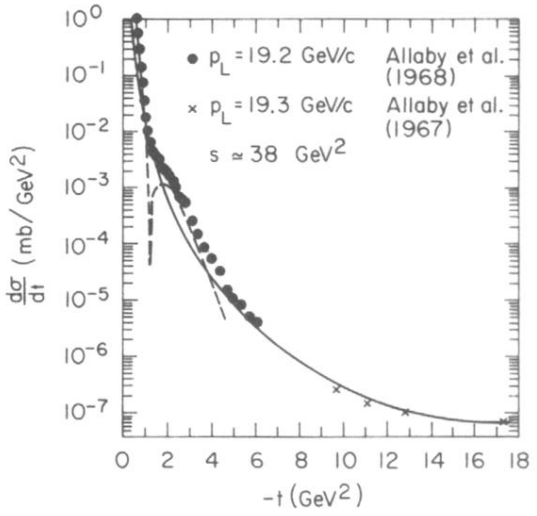

FIG. 15. Differential cross section for pp elastic scattering at $p_L \simeq 19.2$ GeV/c. The solid and dashed lines are the dual and "pure" Pomeron contributions, respectively.

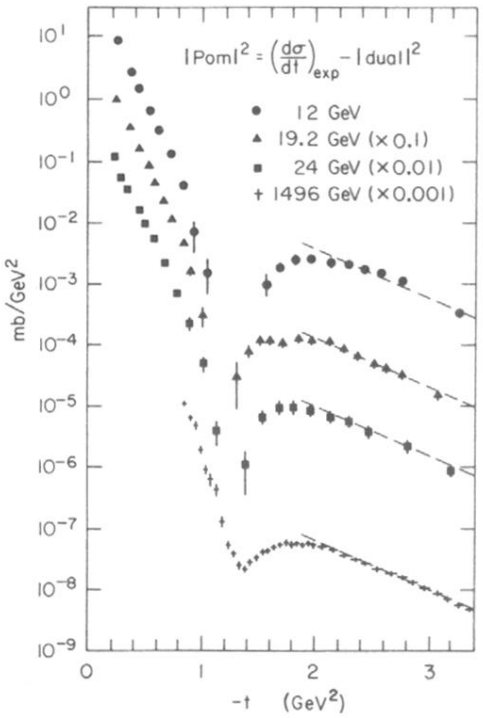

FIG. 16. Pomeron contributions at various energies obtianed by subtracting the dual (normal Reggeon) contribution. Note the dip structure around $t = 1.3$ (GeV)^2 and the same slope for $|t| > 2\,\mathrm{GeV}^2$ at all energies. The solid lines represent a falloff with a slope $A = 1.9$ GeV^{-2}.

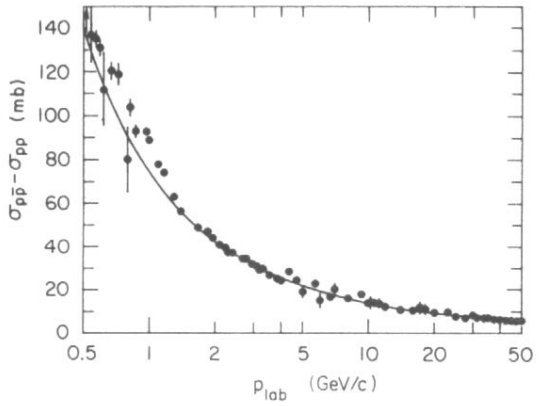

FIG. 17. The solid curve is the dual contribution to $\sigma_{tot}(\bar{p}p) - \sigma_{tot}(pp)$ and the points are values determined from experimental data.

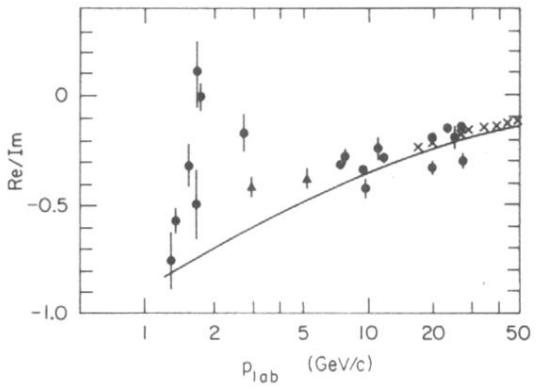

FIG. 18. The solid curve is the predicted ratio of the real to imaginary part of the forward pp amplitude. The imaginary part is computed from the proton-proton total cross section.

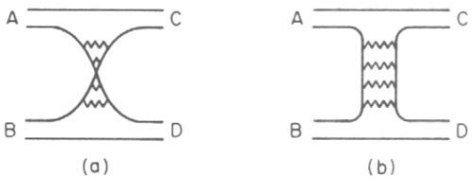

FIG. 2. (a) *ut* and (b) *st* vector-gluon-exchange diagrams which could contribute to Reggeization.

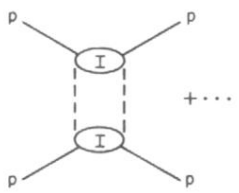

FIG. 3. Illustration of the coupling between $pp \rightarrow pp$ scattering and $p\pi \rightarrow p\pi$ scattering as t-channel iterations become important.

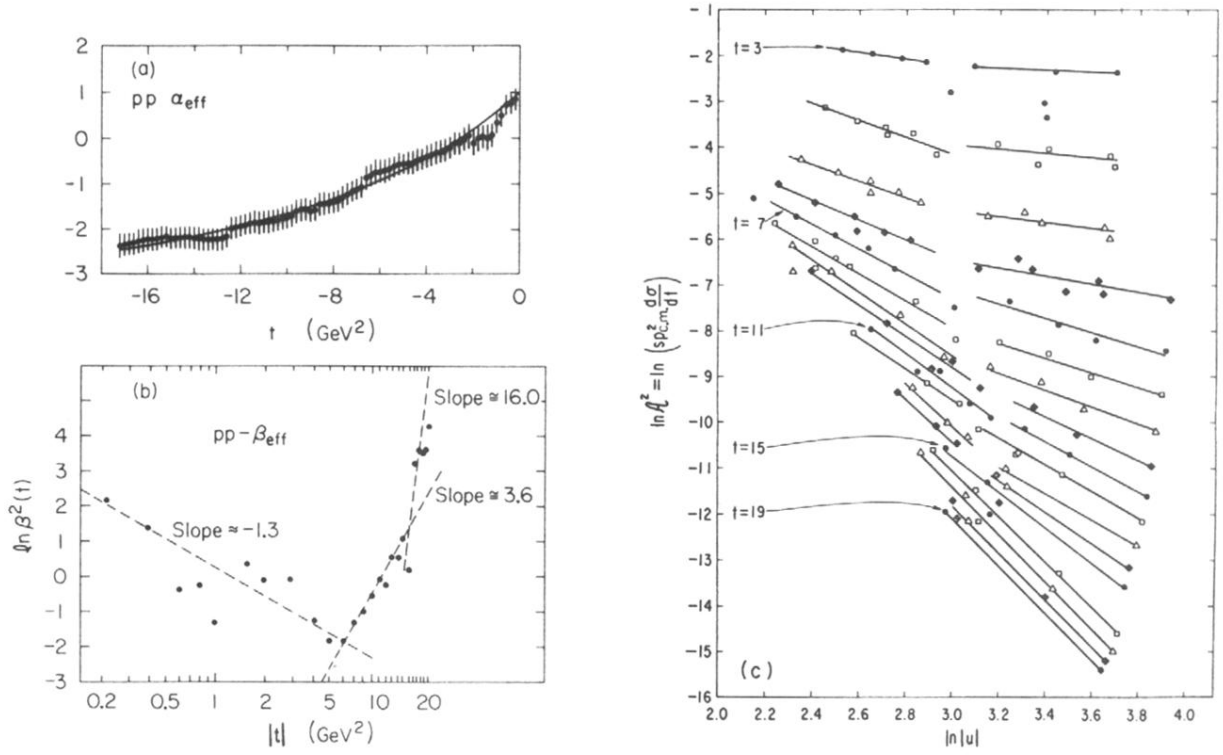

FIG. 4. (a) Extracted effective trajectory for pp elastic scattering. Error bars indicate typical amount of s dependence of extracted α_{eff} at any given t. The variable $(-u)$ is employed. (b) Extracted residue function, $\beta(t)$. (c) Plot of ln $[s^2(d\sigma/dt)]$ vs ln $(-u)$, indicating a possible change in slope (for given t value) as ln $(-u)$ increases.

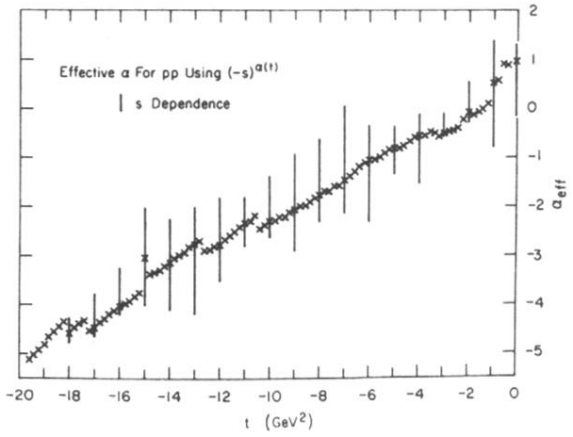

FIG. 5. Extracted effective trajectory using the variable s.

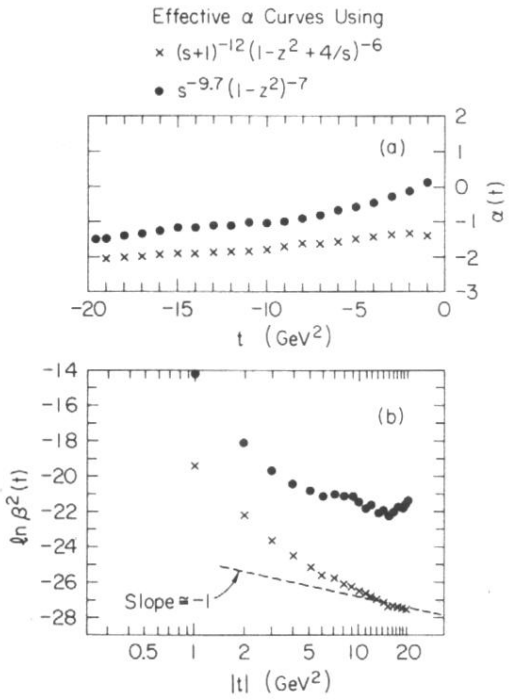

FIG. 6. (a) Effective-trajectory extractions performed using the theoretical cross-section forms of Eq. (12a) (interchange model) and Eq. (13). (b) Extracted residue functions corresponding to the above trajectories.

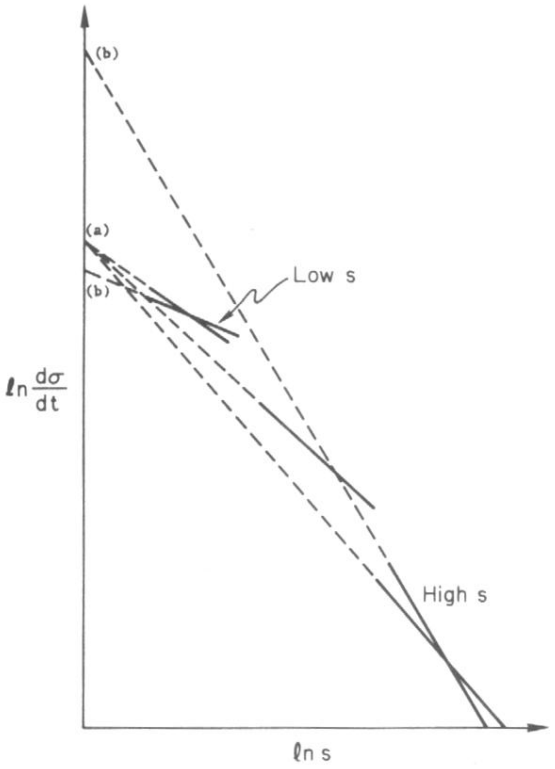

FIG. 7. Rough comparison of cross sections for which (a) the residue function (i.e., intercept on a log-log plot) is constant while the trajectory falls slowly (with increasing $-t$); and (b) the residue function grows as $-t$ increases but the trajectory falls more rapidly in such a way as to *approximately* compensate. The solid portions of the various lines indicate where in ln s the cross section is "measured". These "measurements" are extrapolated back to $\ln s = 0$ to yield either (a), constant residue, or (b), a residue which grows with ln$s$ and correspondingly ln $|t|$. The respective curves are appropriately labeled. We have chosen the intermediate-energy curve to be common to the two cases. Note that the solid-line "measurements" always have a point of overlap.

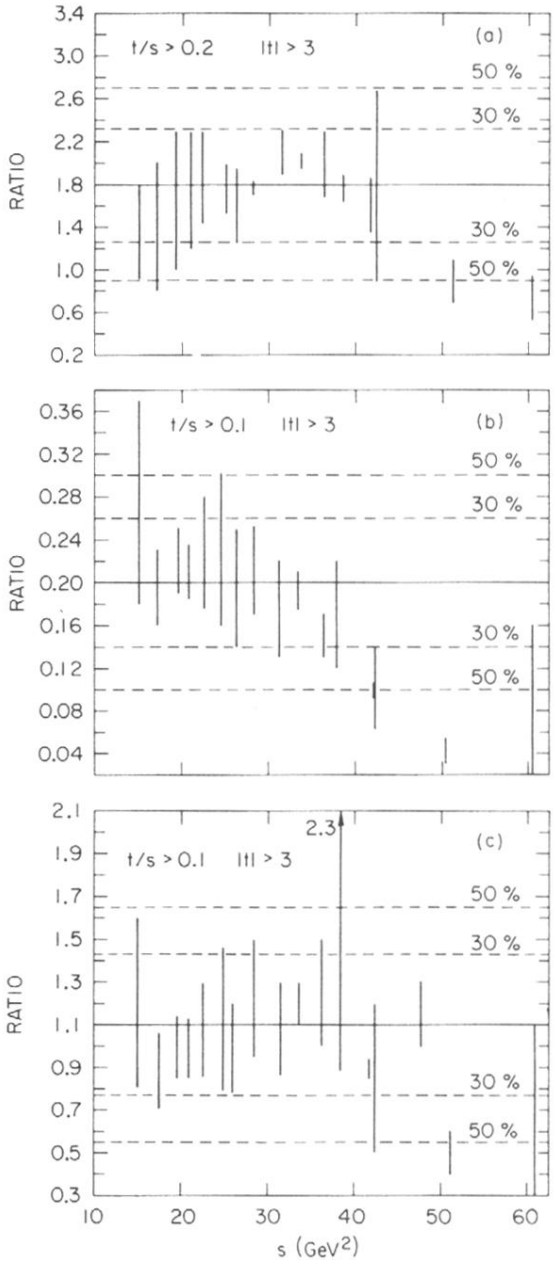

FIG. 8. Plots of the ratio of experimental cross section to theoretical cross section as a function of t for (a) Eq. (12a) (b) Eq. (13) (c) Eq. (12a), modified to have increased $(1 - z^2)$ dependence, $1/(1 - z^2)^7$.

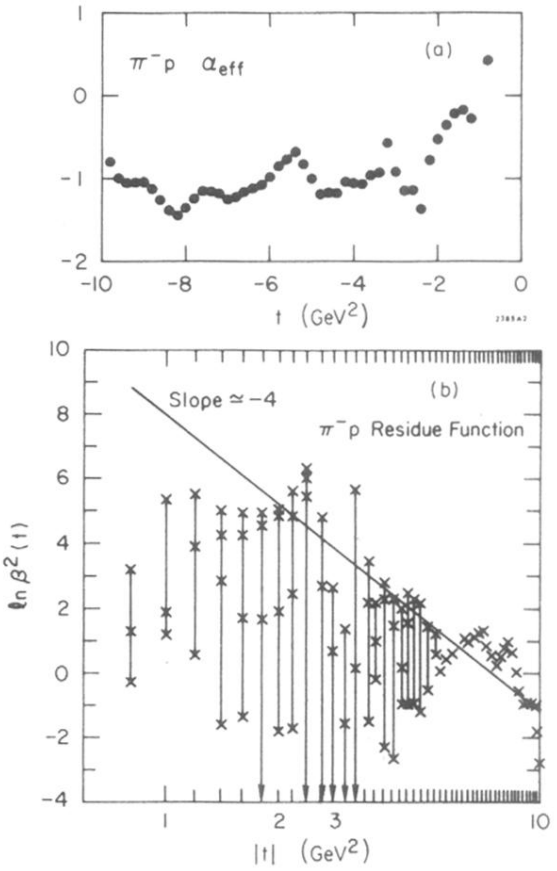

FIG. 9. (a) Effective trajectory for $\pi^- p$ elastic scattering, extracted using Eq. (29). (b) Corresponding residue function. As before error bars indicate s dependence of extracted values: t and $|t|$ in GeV^2.